Commanding variable stiffness in three degrees of freedom through wiggling of a haptic master device.

For a care robot application

J. L. Schol

Delft University of Technology

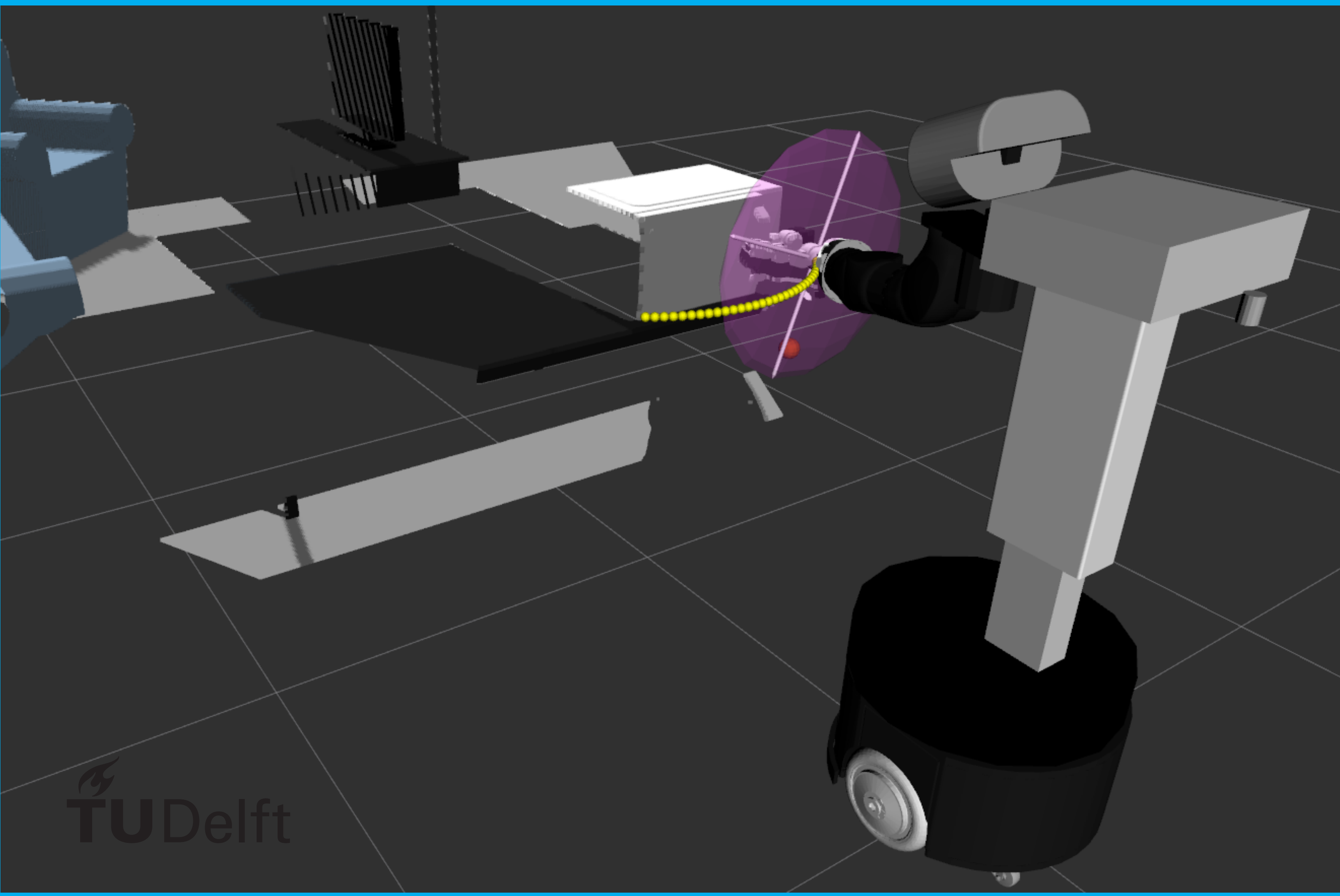

Commanding variable stiffness in three degrees of freedom through wiggling of a haptic master device.

For a care robot application

by

J. L. Schol

to obtain the degree of Master of Science
at the Delft University of Technology,
to be defended publicly on Thursday December 3, 2020 at 13:30 PM.

Student number:	4233646	
Faculty:	Mechanical, maritime and Materials Engineering	
Department:	Cognitive Robotics	
Project duration:	November 1, 2019 – December 3, 2020	
Thesis committee:	Prof. dr. ir. D. A. Abbink,	TU Delft, supervisor
	Dr. ir. L. Peternel,	TU Delft, supervisor
	Ir. J. Hofland,	Heemskerk innovative technology, supervisor
	Dr. ir. C. J. M. Heemskerk,	Heemskerk innovative technology, supervisor
	Dr. ir. C. Della Santina ,	TU Delft, external member

Preface

This work presents the development and evaluation of a novel teleoperated stiffness commanding method in three degrees of freedom. The method aims to enable learning of autonomous manipulation tasks for remote robotic manipulators. The research is inspired by the real-life care robot application where autonomous manipulation tasks could be learned through teleoperated task demonstrations.

Learning from demonstration offers an advantage framework for learning tasks autonomously however, demonstration of kinematic trajectory alone is insufficient to learn complex manipulator-environment interaction tasks. Fortunately, variable impedance control allows regulating the dynamic interaction between the manipulator and the environment through the impedance parameters (stiffness, damping, and/or inertial parameters). By varying the impedance, autonomous manipulation of complex interaction tasks can be achieved. However, demonstration of variable impedance control requires an intuitive system that allows communication of the impedance parameters.

Current systems are limited by the environment or task constraints, lack flexibility in commanding or, are too complex and impracticable for real-life applications. This research tries to overcome these limitations and proposes a system that allows communication of stiffness to a remote manipulator in three degrees of freedom.

The master thesis was submitted in partial fulfillment for the requirements of the MSc Mechanical engineering at the Department of Cognitive robotics, Faculty of mechanical, maritime and materials engineering, Delft University of Technology, The Netherlands. The research was carried out at Heemskerk Innovative Technology (HIT). HIT provided the use case of the care robot application, work environment, and hardware necessary to do the master thesis. The research was conducted under the supervision of Ir. Jelle Hofland and Dr. Cock J. M. Heemskerk of Heemskerk Innovative Technology B.V., and Prof. dr. ir. David A. Abbink and Dr. ir. Luka Peternel of the Department of Cognitive Robotics at the Faculty of Mechanical, Maritime and Materials Engineering.

J. L. Schol
Delft, November 2020

Acknowledgements

Foremost, I would like to thank my supervisors Jelle Hofland, Luka Peternel, David Abbink, and Cock Heemskerk. I would like to thank David for the enthusiasm and ability to always see the essence of the problem during my research. Luka, for the insightful discussions and for sharing your knowledge on a technical level. Both your critical observations and feedback provided me with a better understanding of the research. The monthly meetings did not only helped in providing me direction but after every meeting, the enthusiasm and encouragement truly motivated me to continue working on the project.

Furthermore, would like to thank Jelle, who is always prepared to take the time to understand, assist, and provide guidance on a daily basis. The regular visits offering your help and asking how I was doing is much appreciated (just as the coffee that came along with it). I would like to thank Cock for his knowledge, creative ideas, and never-ending optimism. The biweekly progress meetings helped enormously to keep me focused and I am very grateful to have the possibility to graduate at HIT. Additionally, I would like to thank my fellow students and colleagues at HIT for providing an awesome work environment by means of support, collaboration, and friendships.

Contents

1
Scientific Paper

Commanding variable stiffness in three degrees of freedom through wiggling of a haptic master device.

Jasper Schol[1,2]
Supervised by: Jelle Hofland[2], Cock Heemskerk[2], David A. Abbink[1], Luka Peternel[1]

***Abstract*—Teleoperated semi-autonomous care robots aim to alleviate work pressure from care workers. Unlike many traditional stiff position-controlled robots, the care robot is operating in a shared environment with humans that is often unpredictable and unknown. Especially when dealing with tasks that involve contact with the environment, modulation of compliance is a key component to successfully execute autonomous manipulation tasks. Using Learning from Demonstrating (LfD) techniques, the teleoperator must have a system that allows intuitive demonstration of compliance to the robot. Current state-of-the-art systems are either not teleoperated, only allow limited modulation of the stiffness matrix or, are too complex and cumbersome for practical applications. This research tries to overcome these limitations and proposes a teleoperated stiffness commanding method that allows complete modulation of stiffness matrix in 3 Degrees of Freedom (DoF). The system uses the same haptic device (Geomagic Touch) as used for controlling robot manipulator, hence does not require specialized equipment. Through wiggling the stylus of the haptic device, stiffness is commanded to the robot and directly fed back to the operator through haptic and visual feedback. The system is illustrated in a simulated task where a task appropriate stiffness profile is demonstrated along a kinematic trajectory. Additionally, the performance and acceptance of the system is evaluated through a simulated user study. It shows how varying the commanded DoF, orientation, and size of the stiffness commands significantly influences the performance through the eigenvectors and eigenvalues of the stiffness matrix.**

***Index Terms*—Teleoperation, Haptic interface, Haptic feedback, compliant control, variable impedance control, Varying stiffness, Stiffness commanding, Human-robot interface**

I. Introduction

CURRENTLY, one of Europe's biggest challenge is dealing with a continuously aging society [1]. Throughout the advancement of medical care, the life expectancy grows while the fertility rate declines [2] [3]. This results in more people in need of care while fewer people can provide this. To maintain quality care, there is a need for cost-efficient healthcare solutions.

A potential solution is care robots employed at medical facilities. Equipped with autonomous manipulation skills, the robot assists the healthcare personnel with mundane tasks. However, full autonomous manipulation capabilities for various complex interaction tasks in a dynamic environment are still not feasible. As an alternative, teleoperated robots can deal with a more complex and unpredictable environment and tasks [4]. However, this requires an operator to be present at all times. Therefore, teleoperated robots are only economically feasible when also equipped with reliable and robust autonomous manipulation skills that can handle a large variety of manipulation tasks. Given a certain level of automation, one operator is able to supervise multiple robots making semi-autonomous care-robots an interesting approach.

Traditionally, robots are position controlled. This requires the specification of a kinematic trajectory which is accurately followed by the stiff position controller. In combination with a well organized and known environment, this method excels in repetitive autonomous manipulation tasks such as assembly task in a production line. Care robots on the other hand, are dealing with an environment that is partially unknown, dynamic, uncertain, and shared with humans. Additionally, if the manipulator is interacting or coupled with the environment, pure position control is insufficient [5] as this can lead to excessive forces. Therefore some kind of force control is necessary.

One unique control scheme that can handle various tasks in an unknown environment is impedance control [6]. Impedance control regulates the dynamic interaction between the manipulator and the environment by specifying the kinematic profile and the interactive behavior through impedance parameters (e.g. stiffness, damping, and/or inertial components). Impedance control enables the robot to be robust to uncertainties and increases safety in the form of compliance. Additionally, it does not require a model of the environment and can even be utilized in all manipulation phases and transitions [7]. To even further increase the applicability for various manipulation tasks, impedance can be varied to suit the task at hand. However, when and how to vary the impedance [1] is often specific to the manipulation task.

Given the various tasks the robot could encounter, manual programming of impedance and kinematic trajectories are a tedious and time-consuming approach [8]. As an alternative, reinforcement learning frameworks [9] allow the robot to learn tasks autonomously. However, learning through self-improvement in a feasible time is difficult as it requires a lot of iterations to converge. Moreover, it has the potential to damage the robot without human supervision [10].

[1] *Department of Cognitive Robotics, Faculty of Mechanical, Maritime and Materials Engineering, Delft University of Technology, Mekelweg 2, 2628CD Delft, The Netherlands*
[2] *Heemskerk Innovative Technology B.V., Mijnbouwstraat 120, 2628 RX Delft, The Netherlands*

[1]Generally speaking, impedance can be varied by modulating any of the variables relating force with velocity (e.g. stiffness, damping, and/or mass). In this work, impedance is varied by modulating the stiffness component

Another alternative to manual programming is Learning from Demonstration [11] [12]. In this approach, the operator demonstrates the task while the robot learns based on these demonstrations. This allows for quick and intuitive learning of tasks since the expertise of the operator is captured in the task demonstrations. In the case of impedance controlled manipulators, this requires demonstration of motion and stiffness. As such, the kinematic trajectory can easily be demonstrated by the teleoperator because the robot can record the position from its own sensors [13]. Contrarily, demonstration of stiffness is not trivial as this is a response to an applied force and perturbation. The desired stiffness can not be recorded from the robot sensors or is easily obtainable from human measurements. Therefore, there is a need for an intuitive interface that allows communication of user intended stiffness to the robot manipulator.

Research of [14] [15], do not use a specialized interface to command variable impedance but suggested to use the variability in demonstrated kinematic profiles instead. They related small variability in motion to high impedance and vice-versa. It is hypothesized that small variability in motion requires precise tracking of the reference trajectory which in turn requires a high impedance setting. This method is not flexible since the operator can not control the impedance directly. Therefore, a contact task (e.g constraint motion tasks) will fail since the variability is low, resulting in a high stiffness. This contradicts the desired low impedance to comply with the environment as pointed out in [10].

In [16], the concept of tele-impedance was introduced. Here, surface electromyography (sEMG) measures the muscle activation of the operator. An offline mapping is found that relates the muscle activation to the human arm endpoint stiffness. Using the sEMG to stiffness map, human endpoint stiffness is superimposed to the robot impedance controller to command impedance in real-time. Additionally in [17] [18] [19] force feedback is introduced to this framework and tele-impedance is proven effective in a LfD framework in [20], [21]. However, these methods all require complex offline perturbation-based identification techniques to find the sEMG to stiffness map. The mapping is only locally valid (in the identified arm pose) and operator-specific. Hence new arm configurations or operators require re-calibration, making it unpractical in setup and usage for real-world applications. Additionally, operators are only able to consciously increase stiffness uniform by co-contraction. Other stiffness commands are unconscious and therefore also lack flexibility in commanding stiffness.

Closely related, in [22] sEMG measurements of a single muscle are used to vary the impedance allowing for single DoF commands. This muscle is consciously activated by the operator to regulate the muscle activity that is linearly mapped to the stiffness of the robot impedance controller. Controlling the stiffness through muscle activation heavily relies on the sensorimotor learning ability of the operator [22].

A fundamentally different approach uses grip force as a method to command stiffness. In [23], Walker introduces varying the impedance in 1 DoF based on the force measured by pinching the stylus of the master device. The stylus is equipped with pressure sensors from which the measured force is linearly mapped to the stiffness and damping. Grip force is known to be highly correlated with arm endpoint impedance [24] and therefore considered an intuitive interface.

A slightly different approach is introduced in [10]. Instead of using pressure sensors, a handheld stiffness control interface (potentiometer) is being pressed with the finger to provide stiffness commands in 1 DoF. The methods [22], [23] and [10] are all are limited since the interface only allows single DoF commands. Therefore, the structure of the stiffness matrix (the eigenvectors describing the orientation) must be pre-programmed where only one or multiple eigenvalues can be varied simultaneously. Therefore independent modulation of the eigenvalues is not possible.

In [25] a perturbation based method is used to command impedance to the robot. This technique relies on physically wiggling the robot manipulator around its reference trajectory to modulate the stiffness in the three translational DoF. In [26] this research is extended by combining a method suited to increase the stiffness using pressure sensors. This method requires physical interaction to move the robot. Therefore, remote teaching is not possible. Another limitation is commanding stiffness of large robots hinders physically perturbing the robot. Finally, environment constraints can prevent the manipulator to be moved in a certain direction which can only be solved by commanding the robot with an offset in trajectory [26]. Nevertheless, this method does provide the possibility to vary both the eigenvectors (direction) and eigenvalues (magnitude) of the stiffness matrix providing a lot of flexibility in modulating the stiffness.

Different methods for demonstrating variable impedance are reviewed. It is shown that current state-of-the-art methods are not versatile since they, do not allow for (flexible) conscious stiffness commands [14], [15], [16], [27], [18],[20],[19]. Additionally, the methods [22],[10],[23] are not flexible since they only allow modulation of a single eigenvalue (or multiple simultaneously) for a pre-programmed structure of the stiffness matrix. Therefore stiffness commands that vary 2 DoF independently are not possible. Moreover, tasks that require directional changes of stiffness require additional programming of the structure of the stiffness matrix along the trajectory. The methods mapping the muscle activation to endpoint stiffness are considered impractical due to their complex calibration procedure and setup time [16], [27], [18],[20],[19]. Finally, the methods [25],[26] are not teleoperated. It can be concluded that current state-of-the-art impedance commanding techniques lack a flexible and practical teleoperated stiffness commanding interface, suited for learning impedance behavior for various tasks in 3 DoF.

Given the limitations of the existing methods, this work proposes and evaluates a teleoperated stiffness commanding interface that allows the operator to consciously provide a varying stiffness profile in 3 DoF. Where the three translational DoF can be varied in the direction (eigenvectors) and magnitude (eigenvalues). To make the interface suited for a real-world practical application, it is also important that the interface is low-cost and allows for easy implementation on various platforms. Therefore demonstration of stiffness should not be dependent on the environment (constraints), robot, or the kinematic robot trajectory. Additionally, the interface must be accepted by the operator such that stiffness behavior can be easily and intuitively programmed.

Similar to [25] and [26] this method uses perturbations around the kinematic reference trajectory in order to provide stiffness commands. Different from these works is that the perturbations are not introduced by physically wiggling the robot. In this work, the haptic master device (Geomagic touch) is used to make the virtual perturbations. During a simulated trajectory execution, the operator is moving a virtual marker around the current end-effector position of the robot. The operator wiggles the stylus of the haptic device thereby moving the virtual marker away from the current end-effector position. The larger distance between the virtual marker and the end-effector (amplitude), the lower the stiffness, and the more compliant the end-effector of the robot will become in that direction. The commanded stiffness is updated online and fed back to the operator through a compliance ellipsoid visualization, and by providing virtual stiffness forces from the haptic device. Therefore, the operator sees and feels the stiffness change what helps evaluating to which extend the commanding is successful. After the stiffness profile is demonstrated in simulation, the robot could use the obtained stiffness profile in order to autonomously execute the task in real-life.

The contributions of this research are:

1) A Teleoperated stiffness commanding method that allows conscious modulation of the stiffness matrix through the eigenvalues and eigenvectors for 3 translational DoF.
2) A user study that evaluates the performance and acceptance of the proposed stiffness commanding interface in simulation.
3) A Demonstration of the stiffness commanding method in simulation illustrating the applicability for real-world tasks.

II. Methods

The main objective of the stiffness commanding system is varying the stiffness parameter of an impedance controller. The concept of varying stiffness can be used for any kind of compliant control such as impedance control or even admittance control (impedance control with inner position control loop) [5]. The only requirement is a stiffness component present in the controllers model equation. In Fig. 1 a system overview is presented containing the most important software blocks, signals, and apparatus.

This work assumes an already established kinematic trajectory x_c and no assumptions are made on how this is obtained. Additionally, during the stiffness demonstration in simulation, the impedance controller is temporarily bypassed to facilitate the creation of the stiffness profile. For a real-life task execution, the impedance controller would use the demonstrated stiffness profile to autonomously execute the task. Note, that it would also be possible to command stiffness directly during the real-life motion execution however, incorrect stiffness commands could potentially damage the robot when in contact with the environment.

Part of the impedance controller implementation given in the Appendix A.4. Furthermore, it shows how the general impedance model equation relates to a torque controlled robot along with a more complete system overview as presented in Fig. 1.

A. *Stiffness commands from perturbations*

The stiffness commanding method is intended to command stiffness for the 3 translation DoF. Therefore, the stiffness matrix $\mathbf{K} \in \mathbb{R}^{3\times 3}$ relates the contact forces to position errors. The stiffness matrix K is found, by setting it inversely proportional to a coveriance matrix. This covariance matrix is constructed based of a perturbation signals that is created by the operator moving the stylus. By wiggling a virtual marker point $\mathbf{x_m} \in \mathbb{R}^{3\times 1}$ around the current robot end-effector position $\mathbf{x} \in \mathbb{R}^{3\times 1}$, a perturbation vector can be found for each time step.

$$\boldsymbol{\tilde{x}_i = x_i - x_{m,i}} \tag{1}$$

The perturbation vector is stored over time in a data matrix $\boldsymbol{\Xi^{\tilde{x}\times L}}$. From this data matrix, a covariance matrix $\boldsymbol{\Sigma_i} \in \mathbb{R}^{\mathbf{3\times 3}}$ is constructed. Here $L = dt{\times}T = \frac{T}{f_s}$ is the total amount of stored data points in the data matrix and hence the length of the sliding temporal window. Where $T\ s$ is the time span of the window and f_s the frequency at which the software runs. As time progresses with time step dt, a new perturbation vector will be appended while the earliest vector will be removed from the data matrix. Therefore at time $t = t_1$, the data matrix contains the perturbation vectors in the range $|(t_1 - T),\ t_1|$ for $t_1 > T$. From this data matrix, the symmetric and positive definite (SPD) covariance matrix is found according to

$$\begin{aligned} \boldsymbol{\Sigma_i} &= \boldsymbol{\frac{1}{L}\sum_{i}^{L}(\tilde{x}_i - \mu)(\tilde{x}_i - \mu)^T} \\ \boldsymbol{\mu_i} &= \boldsymbol{\frac{1}{L}\sum_{i}^{L}\tilde{x}_i} \end{aligned} \tag{2}$$

where $\boldsymbol{\mu}$ is the average of the perturbation vectors in the data matrix. The three variances corresponding to the x,y and z-axis are presented on the diagonal of the covariance matrix and the of-diagonal elements represent the covariance (coupling terms) between x,y and z-axis. The next step is to set the covariance matrix inversely proportional to the stiffness matrix. Therefore, the direction and the magnitude should be found. Since the covariance matrix is a SPD matrix, eigendecomposition gives

$$\boldsymbol{\Sigma_i = Q\Lambda Q^T} \tag{3}$$

where $\boldsymbol{Q} \in \mathbb{R}^{\mathbf{3\times 3}}$ is a matrix containing the orthonormal eigenvectors (direction) and $\boldsymbol{\Lambda} \in \mathbb{R}^{\mathbf{3\times 3}}$ is a diagonal matrix composed of the eigenvalues $\lambda_i,\ i = 1, 2, 3$ (magnitude along the eigenvectors). From (3) we keep the eigenvectors and use this to construct the stiffness matrix

$$\boldsymbol{K = Q\Gamma Q^T} \tag{4}$$

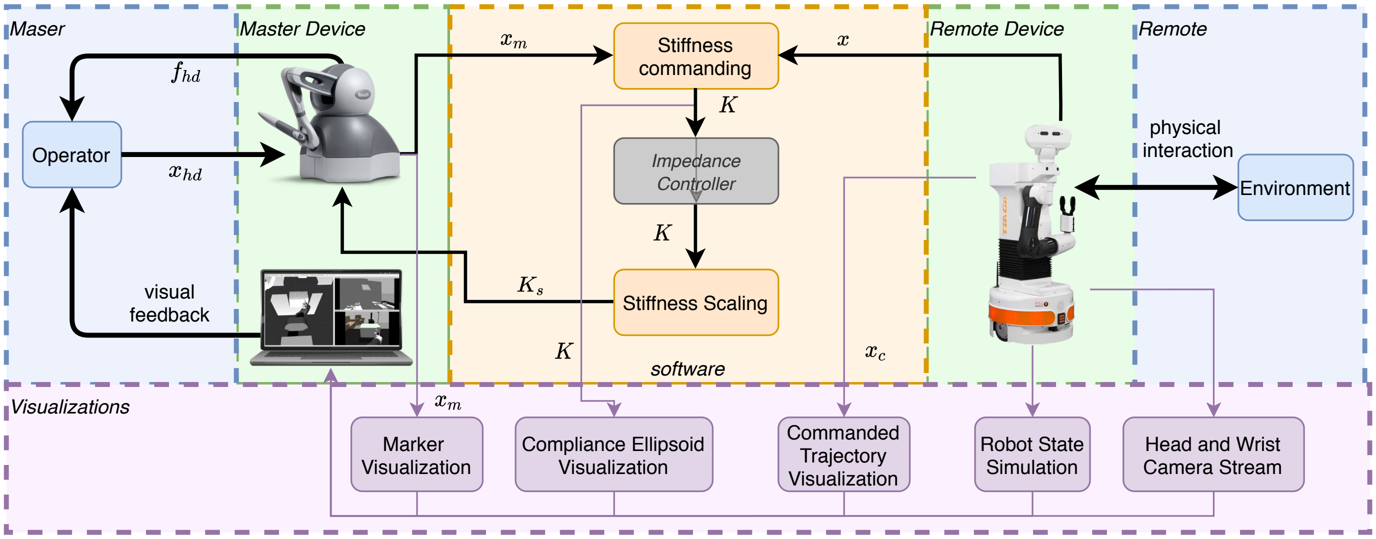

Fig. 1. System overview containing the most important software blocks, signals, and apparatus. The operator and the remote environment (blue sections) interact with the master and remote devices respectively (green sections). The yellow section contains the software blocks and signals and the purple section shows the visualization based of the important signals or robot sensors. Since no impedance (compliant) controller is implemented, the stiffness command K is directly connected to the stiffness scaling. A more complete system overview including impedance controller is given in Appendix A.4

where $\mathbf{\Gamma}$ is a diagonal matrix of which the diagonal elements γ_i are defined to be the inverse to the square root of the diagonal elements of matrix $\mathbf{\Lambda}$, such that $\sigma_i = \sqrt{\lambda_i}$. The inverse relation for each diagonal element $\gamma(\sigma_i)$ is given by

$$\gamma(\sigma_i) = \begin{cases} \underline{K} & \sigma_i > \bar{\sigma} \\ \bar{K} - \frac{\bar{K}-\underline{K}}{\bar{\sigma}-\underline{\sigma}}(\sigma_i - \underline{\sigma}) & \underline{\sigma} \leq \sigma_i \leq \bar{\sigma} \\ \bar{K} & \sigma_i < \underline{\sigma} \end{cases} \tag{5}$$

where σ_i is a measure of the amplitude of the perturbations (wiggles) where the minimal and maximal allowed perturbations $\underline{\sigma}$ and $\bar{\sigma}$ are a tunable parameters. Since the diagonals of $\mathbf{\Gamma}$ (γ_i) should be bounded between the stiffness limits of the impedance controller, the stiffness diagonal γ is set inversely proportional to the perturbations measure σ. Therefore, the minimal and maximal allowed perturbation $[\underline{\sigma},\ \bar{\sigma}]$ is related to the minimal and maximal allowed stiffness limits of the impedance controller. The minimal and maximal stiffness is denoted by $[\underline{K},\ \bar{K}]$.

B. Visual feedback

Since stiffness commands are given using a teleoperated setup, it is important to have a good understanding of the remote robot and the environment. Additionally, to understand the system itself visual cues are known to improve user acceptance and performance in Haptic Shared Control systems [28] [29].

In Fig. 2 the operators screen is divided in 3 sections. The right side shows at the top a camera stream from the robot's head camera, and at the bottom the end-effector camera stream. The left side of the screen provides a simulated environment based of robot sensors. Here, the current robot state and additional visualizations of the signals are presented. The figure also shows the task of opening a microwave door.

The simulated environment includes a model of the current robot state 1) and a point cloud 2) that shows the environment constructed from the depth camera. In the simulated view, the commanded end-effector trajectory 3) is visualized helping in understanding the End-effector its future motion. The virtual marker 4) is presented by the red sphere that is controlled by the stylus of the haptic device. By moving the marker away from the end-effector, the marker color gradually changes from green to red providing a sense of depth. Finally, the compliance ellipsoid 5) is used to visualize the stiffness commands and help operators understanding the effect on the stiffness from the input stylus motion commands. Although the compliance ellipsoid is the inverse of a stiffness ellipsoid, the choice is made to visualize compliance since this naturally matches the movement of the virtual marker x_m. For example, if the operator wiggles the stylus along the z-axis, the compliance ellipsoid forms a cigar shaped ellipsoid with the long axis aligned with the z-axis. This is intuitive since the long axis forms in the line of movement from the wiggling motion resulting in lower stiffness along the z-axis. The implementation of the compliance ellipsoid visualization is given in Appendix A.5.1.

C. Haptic feedback

Normally in teleoperation, the haptic feedback of the master device is used to make the manipulator inertia observable, or to provide feedback forces from manipulator-environment contact.

This research however, uses a different method to provide haptic feedback. In this work, the commanded manipulator stiffness is explicitly made observable through the haptic device by scaling the commanded stiffness and using this to produce a virtual stiffness force. If the stylus moves away from its zero position, the virtual stiffness force pulls it back to the zero position similar as how an impedance

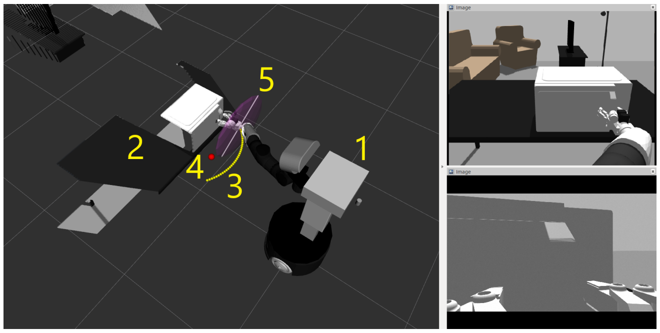

Fig. 2. Visuals as provided to the operator. The left side shows a simulated view as constructed from the robot sensors including additional visual ques. The top right and bottom view are the head and wrist camera streams that show the real (in this case simulated) world. The task mimics the process of opening the door of a microwave.

controlled manipulator would move back to its equilibrium trajectory. Therefore, the operator can sense the effects of the commanded stiffness directly without an actual impedance controller being present. This allows commanding of stiffness even for simulated motion where contact forces are absent. Since the operator evaluates the stiffness directly, it allows for quick adjustments during the motion. Additionally when a fixed stiffness is set (e.g. from earlier demonstrations), it also allows users to feel and improve upon the earlier commanded stiffness. It is important to convey this information haptically since this is how people naturally evaluate stiffness [25]. Furthermore, it supplements the compliance ellipsoid visualization since it can be seen and felt simultaneously.

The virtual stiffness force is calculated by multiplying the scaled-down manipulator stiffness $\mathbf{K_s} \in R^{3\times 3}$ with the stylus deviation from its zero position. To set (or limit) the force the haptic device can produce (Geomagic Touch maximal force output is 3.3 N), the stiffness should be scaled to ensure that the haptic device uses the full or a defined range of force. This is done by defining the maximally allowed deviation $\bar{x}_{hd}$ of the stylus and the minimal and maximal force limits (for maximal stylus deviation). $[\underline{f}_{hd},\ \bar{f}_{hd}]$ of the haptic device. Subsequently, the minimal and maximal allowed stiffness for the haptic device for maximal stylus deviation is defined as

$$\underline{K}_{hd} = \frac{\underline{f}_{hd}}{\bar{x}_{hd}} \qquad \bar{K}_{hd} = \frac{\bar{f}_{hd}}{\bar{x}_{hd}} \tag{6}$$

By relating the minimal and maximal manipulator stiffness limits $[\underline{K}.\ \bar{K}]$ to the minimal and maximal allowed haptic device stiffness limits, the scaled down stiffness can be found.

In order to scale the stiffness matrix $\mathbf{K}$, eigenvalue decomposition of the stiffness matrix has to be performed such that the eigenvalues can be scaled. Using the eigenvalues of (4), the diagonal matrix with the scaled eigenvalues $K_{s,e}$ is given by

$$\mathbf{K_{s,e}} = \underline{\mathbf{K}}_{\mathbf{hd}} + \frac{\bar{K}_{hd} - \underline{K}_{hd}}{\bar{K} - \underline{K}}(\mathbf{\Gamma} - \underline{\mathbf{K}}) \tag{7}$$

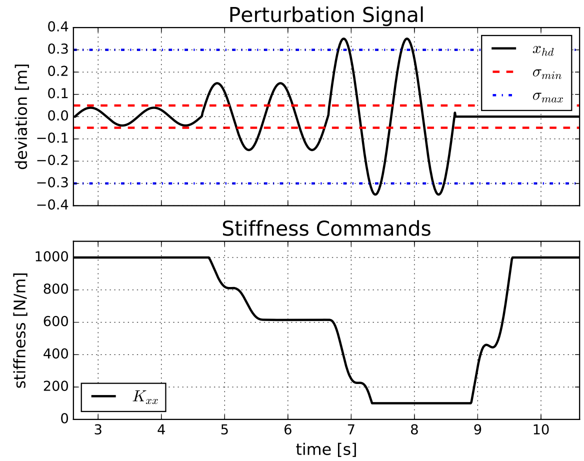

Fig. 3. The top plot shows a sinusoidal perturbation signal along the x-direction and the bottom plot shows the resulting stiffness commands.

where $\underline{\mathbf{K}}_{\mathbf{hd}}$, $\underline{\mathbf{K}}$ and $\bar{\mathbf{K}}$ are diagonal matrices with on the diagonals $\underline{K}_{hd}$, $\underline{K}$, $\bar{K}$ respectively. Once again, using (4) the scaled stiffness matrix is found using the eigenvectors of the decomposition.

$$\boldsymbol{K_s} = \boldsymbol{Q}\boldsymbol{K_{s,e}}\boldsymbol{Q^T} \tag{8}$$

Subsequently, the force feedback is calculated by

$$\boldsymbol{f_{hd}} = \boldsymbol{K_s}\boldsymbol{x_{hd}} \tag{9}$$

where $\boldsymbol{f_{hd}}$ is the virtual stiffness force produced by the haptic device and $\boldsymbol{x_{hd}}$ is the stylus deviation away from the zero position.

D. Stiffness behaviour

This section shows how the perturbation signal (operator input) influences the stiffness commands and how the tune parameters influence the system. Given the stability stiffness limits of the manipulator, parameters that influence the stiffness commands are the amount of data points in the sliding window $L = dt \times T = \frac{T}{f_s}$, and the parameters $\bar{\sigma}$, $\underline{\sigma}$. The sliding window length along with the frequency rate of the software determines the time it takes to completely refresh the window with data points. The time it takes to refresh the window mainly influences the rate of change of stiffness. Therefore, a large window and a high frequency rate corresponds to slow rate of change of stiffness and vice-versa. The parameters $\underline{\sigma}$, $\bar{\sigma}$ represent the standard deviation of the data in the data matrix $\mathbf{\Xi^{\tilde{x}\times L}}$ and are related to minimal and maximal allowed deviation of the haptic device stylus. Given the inverse relation of (5), motion below $\underline{\sigma} = 0.0707$ increases the stiffness to the maximum limit $\bar{K} = 1000\ N/m$ and above $\bar{\sigma} = 0.3$ to a minimum limit $\underline{K} = 100\ N/m$ of the manipulator. This effect is shown in Fig. 3.

The sliding window length and software frequency are $L = 100$ and $f_s = 100\ Hz$. Therefore, the time it takes to complete refresh the window is $T = 1\ s$. This can be observed by looking at the top and bottom subplots of Fig. 3. At the top plot at approximately 4.5 s a sinus with an amplitude larger than the threshold starts. After 1 second the window is completely refreshed with new data points and this shows in the bottom plot where the stiffness has flattened to 600 N/m at 5.5 s.

Furthermore, in Fig. 3 small bumps are observed during the in and decrease of the stiffness signal. This can be explained by the peaks of the perturbation signal. Around the top of the peak, the direction of movement changes resulting in more data points around that position. These points temporarily lower the variance of the covariance matrix which is directly related to an increase in stiffness. More effects of the influence of the perturbation signal (noise, frequency, and window length) on the stiffness as given in Appendix A.5.

E. Task demonstration

The purpose of this task demonstration is to illustrate that the proposed method can command stiffness variations along a trajectory for a real-world task. The task demonstration runs in gazebo where the robot and the environment are simulated. The operator is presented with the screen containing the visualization and camera streams. The task mimics a door opening task of a microwave as shown in Fig. 2. The task involves an approaching phase and an opening phase where the complete trajectory along with the compliance ellipsoids are visualized in Fig. 4a.

At the end of the approaching phase, the robot is required to be maximally compliant in the direction of the microwave handle to prevent high impact forces. The remaining directions are required to be maximally stiff such that the gripper is accurately positioned at the handle. During the approaching phase, the stiffness commands are provided in 1 DoF by wiggling along the x-direction of Fig 4a.

For the opening phase, the manipulator should be stiff in the direction of movement to overcome the force needed to open the door. The other two directions should be maximally compliant such that the end-effector complies with the constrained motion of the door. This allows the robot to deviate from the programmed trajectory when it does not perfectly match the real-world trajectory of the door handle. This prevents the robot from getting stuck or even damaging the microwave or robot. The 2 DoF stiffness commands are given by creating a circular motion around the outer edge of the compliance ellipsoid. Between the approaching and opening phase, the trajectory is paused and the stiffness profile should be changed as quickly as possible.

In Fig. 4b the diagonals and eigenvalues of the stiffness matrix are plotted. The stiffness matrix is presented in the end-effector frame where the end-effector remains perpendicular to the handle of the microwave. Ideally, at 3.6, s the diagonal component K_{xx} should therefore be maximally compliant. Similarly, between $4.7 - 11$ s the components $K_{yy},\ K_{zz}$ should be maximally compliant. The stiffness eigenvalues show that at approximately 3.6 s maximal compliance of $\gamma_1 = 100\ N/m$ is reached. The corresponding matrix diagonal $K_{xx} \approx 150\ N/m$ is slightly higher. This can be explained by the error in the orientation of the compliance ellipsoid. Therefore, the impact forces in the x-direction would be slightly higher than intended. When changing from a cigar-shaped ellipsoid to a circular-shaped ellipsoid, it roughly takes around 1 s which is the minimal time for the defined $L = 100$ and $f_s = 100\ Hz$ to switch between the saturation stiffness limits. Between $5 - 10$ s the stiffness diagonals are close to the intended limits. Similar to the approaching phase, the stiffness diagonals between $10 - 11$ s deviate from the intended limits because of an orientation error. Therefore, the circular-shaped compliance is not perpendicular to the motion of the end-effector. At 11 s, the stiffness commands are stopped.

III. EXPERIMENTAL METHOD

The previous section describes the working principles of the stiffness commanding method along with a task demonstration that illustrates how the interfaces can be used for a real life task. An important aspect of the method is that non-experts operators can conveniently use this, such that it can be incorporated in a LfD framework. In this section, the method is evaluated through a user study. In the experiment, the operator is instructed to recreate various compliance ellipsoid (representing the stiffness matrix) as accurately as possible. The trials are evaluated on trial time, and by comparing the operator commanded ellipsoid with the reference ellipsoid. The reference ellipsoids are varied in size, orientation, and require either 1 or 2 DoF commands. The purpose of the experiment is twofold. First, to evaluate how well the operator can command stiffness variation. The performance is analyzed within the method itself and tries to identify how the performance is influenced by the different conditions. Secondly, to evaluate the user acceptance by using the *van der Laan* questionnaire [30]. This simple procedure measures the self-reported satisfaction and usefulness of the stiffness commanding interface.

It is hypothesized that single DoF stiffness commands will have higher performance scores, compared to 2 DoF stiffness commands. A theoretical model is used to describe task complexity in [31]. This model implies that the required acts needed for the creation of a product contributes to the overall task complexity. Furthermore, depending on the individual capacity, a high level of task complexity exceeds the individual capacity which leads to lowered performance. The act for the creation of a 2 DoF stiffness ellipsoid requires controlling the magnitude and orientation along more axes compared to commands in 1 DoF. Therefore, the task performance is hypothesized to be lower in 2 DoF.

Secondly, it is hypothesized that commanding compliance in the horizontal (or transverse) plane will have lower performance scores as compared to commands in the vertical (or frontal) plane. The reason being that commands in the horizontal plane requires the operator to predominantly use a screen that has a top-down view of the horizontal plane. Therefore, misalignment exists between the operator view and the control input which does not exist in the vertical plane. In [32] it is shown that to improve teleoperation, a setup should minimize control and view rotations. Additionally, the manipulability of the human arm is different in the horizontal plane as compared to the vertical plane through the pose of the arm. No research is found that directly relates the effect of human arm manipulability for different planes on teleoperated

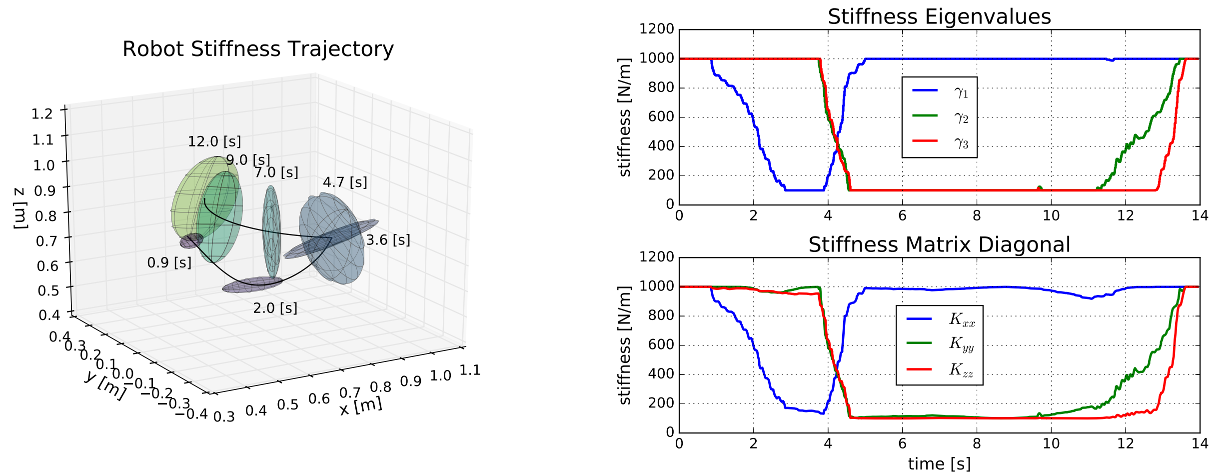

(a) (b)

Fig. 4. On the left (a), the compliance ellipsoids are visualized along the robot trajectory. The trajectory mimics the approach ($0 - 3.6\ s$) and opening ($4.7 - 11.0\ s$) phase of a microwave (see Fig. 2). The right (b), shows the corresponding eigenvalues of the stiffness matrix and the diagonal elements of the stiffness matrix. The stiffness matrix is represented in end-effector frame.

task performance however, it could contribute to performance in or decrease.

Finally, it is hypothesized that larger shapes take more time to command compared to small shapes. To create large shapes, the stylus has to travel a greater distance resulting in more time needed per trial. No effect is expected in terms of similarity between the reference and user commanded stiffness ellipsoid.

A. *Participants*

The study uses a within-subject design where every participant tests all the conditions. Eight male participants aged $M = 25.15, SD = 2.53$ volunteered and were included in the experiment. All participants have an engineering background of which 4 participants have reported having at least ten weeks of teleoperation experience in any field. One participant has 1 week of teleoperation experience and the remaining three participants have between 1 and 10 hours of teleoperation experience. Prior to the experiment, all participants gave their consent and the experiment is approved by the Human Research Ethics Committee of the Delft University of Technology. The experimental procedure and forms are given in Appendix G.

B. *Experimental setup*

The experiments were performed on a telemanipulation setup consisting of a Geomagic Touch and a computer screen. The Geomagic touch allows providing of 6 DoF pose (translation/orientation) inputs and provides force feedback in the 3 translational DoF. Only the 3 translational DoF position commands and force feedback are used in the experiment. The computer screen provides two views. The upper part of the screen provides a top-down view of the horizontal plane, while the bottom part of the screen provides a frontal view of the vertical plane. The experiment and software are implemented using ROS and visualized in RVIZ. The experiment visualization is presented in Appendix B.3.

C. *Experiment protocol*

Before starting the experiment each participant was provided a description of the interface, task, and task instructions as presented in Appendix H. Next, the participants were allowed to familiarize themselves with the setup to understand how their perturbations affected the compliance ellipsoid. After 5 minutes of familiarization time, the participants had to reach a minimum score for 12 trials in which all conditions were presented. All participants passed within 1 or 2 tries and advanced to the experiment.

In the experiment, the participant had to command in four different conditions where each condition was preceded with a practice run to get used to that specific condition. After each condition, the participants were asked if they had any problems during the experiment and if they had any comments. During the experiment only questions regarding safety or clarification of experiment instructions/ protocol were answered. After the final condition, the participants were asked to fill in a *van der Laan* questionnaire along with four questions complementing the questionnaire which is given in Appendix I. The questions are:

- What did you like or found helpful?
- What did you find undesirable or hard?
- Which condition did you find most difficult and why?
- Do you have any remarks?

D. *Experiment design*

The conditions vary in 1 or 2 DoF stiffness commands and spawn the compliance ellipsoids in a horizontal or vertical plane. The conditions are:

- 1 DoF – horizontal

- 1 DoF – vertical
- 2 DoF – horizontal
- 2 DoF – vertical

Every participant started with a 1 DoF condition followed by the 2 DoF condition of the same plane. The planes are counterbalanced where half the group started with horizontal commands and the other group started with vertical commands.

Within each condition, the ellipsoids are varied in size (small, large) and orientation ($0, 45, 90, 135$ deg). The 1 DoF reference ellipsoids have one long axis of which the size is varied to be either large (0.46) or small (0.25) forming the shape of a "cigar". The 2 DoF ellipsoids have the same long axis in addition to a second axis that is half the size of the long axis. These two axes form an "oval" in the plane of their corresponding condition. Both 1 and 2 DoF ellipsoids are rotated in their plane with either $0, 45, 90, 135$ deg. Within each condition, every combination of size and orientation is repeated four times. The 2 DoF conditions have two additional ellipsoids, a small and large "circle" which are both repeated four times. They are not rotated since all orientations result in the same compliance ellipsoid.

The metrics are used to measure the performance of the participants for the individual trials, and to provide feedback to the operator during the experiment. The metrics evaluate the trial time and the similarity between the stiffness matrix. The similarity is evaluated by decomposing the stiffness matrix in a orientation (eigenvectors) and size (eigenvalues) component according to (4). Thus, the error between the reference and the commanded ellipsoid is evaluated by comparing the eigenvalues and eigenvectors. The decomposition of the stiffness matrix allows for a physical interpretation of the compliance ellipsoid (i.e. stiffness matrix). Moreover, it allows evaluating which part (orientation and/or size) influences the performance, for the given various conditions. Therefore, more precise observations can be made in order to evaluate and improve the method.

Trial time – Is defined to be the time it takes for the participant to recreate the reference ellipsoid in seconds. The time starts as the new reference ellipsoid spawns and is stopped by the operator when a satisfactory performance was reached. This is done by the press of a button which also automatically spawns the next reference ellipsoid. High trial times correspond to lower performance and vice versa.

Absolute average size error, s – Is defined to be the average of the absolute error between the reference and the operator commanded ellipsoid axes.

$$s = \frac{1}{n}\sum_{i=1,2,3}^{n} |\sigma_{ref,i} - \sigma_{com,i}| \tag{10}$$

Relative average size accuracy, s_{acc} – Is defined to be the average error between the reference and the operator commanded ellipsoid axes, relative to the reference ellipsoid. Additionally, the score is converted to a percentage such that it can be presented to the operator as a convenient feedback score during the trials. The score ranges between $0 - 100\%$ where 100% represent a perfect match in size.

$$s_{acc} = 100 - \frac{1}{n}\sum_{i=1,2,3}^{n} \left\{ \frac{|\sigma_{ref,i} - \sigma_{com,i}|}{\sigma_{ref,i}} \times 100 \right\} \tag{11}$$

Orientation error, α – Using the axis angle definition, α is defined to be the smallest absolute angle between the reference orientation and the user commanded orientation for an arbitrary axis. The absolute angle is derived from a distance metric for 3D rotations: the inner product of a unit quaternion ϕ [33].

$$\phi = \arccos\left(|\mathbf{q_{ref}} \cdot \mathbf{q_{com}}|\right) \tag{12}$$

The distance metric ϕ is scaled by a factor of 2, to represent the angle in radians. Subsequently, the range is halved to $[0 - \frac{\pi}{2}\ rad]$ because of the symmetry of the ellipsoid.

$$\alpha = \begin{cases} \pi - 2\phi & 2\phi > \frac{\pi}{2} \\ 2\phi, & \text{otherwise} \end{cases} \tag{13}$$

The angle α is also represented as a feedback accuracy score α_{acc} to the operator in (14). Similar as to the size accuracy, 100% represents a perfect match in orientation. The feedback score is identical to α only scaled to have a different range $[0 - 100\%]$

$$\alpha_{acc} = 100 - (\alpha\frac{2}{\pi} \times 100) \tag{14}$$

During the experiment, the operator receives feedback from their orientation accuracy (14) and size accuracy (11) for every trial. The feedback scores are color-coded in red, orange, and green representing low, medium, and high scores respectively. The participants were instructed to aim for green scores and avoid red scores.

IV. Experimental Results

The experiment compares the performance on commanded DoF (1 versus 2), plane (horizontal versus vertical), and size (large versus small) and are presented in Table I. The most important quantitative and subjective results are visualized in Fig. 5.

The complete data sets consist of 512 trial pairs for the DoF conditions and 576 pairs for the Plane and Size conditions. In the DoF data set, the 2 DoF "circular-shaped" ellipsoids are removed in order to fairly compare with the 1 DoF data set. Therefore, the 1 DoF "cigar-shaped" ellipsoids are compared with the 2 DoF "oval-shaped" counterpart. Since the 2 Dof "circles" do not have a representative pair in 1 DoF, circles are omitted. Additionally, some trials and their corresponding pair are removed based on accidental trial advancements or skipped trials. The individual data sets are checked on a normal distribution using the Shapiro-Wilk test [34] and subsequently tested on logistic and Gumbel distributions using the Anderson-darling test [35], [36]. None of the results are significant. Therefore, the data is tested using the nonparametric Wilcoxon signed-rank test [37]. The test compares the medians between the conditions and results are considered statistically significant when $p \leq 0.05$.

TABLE I

THE DESCRIPTIVE STATISTICS (LEFT) SHOW THE MEDIAN (Q_2), FIRST QUARTILE (Q_1), AND THIRD QUARTILE (Q_3) OF THE DATA SETS. THE INFERENTIAL STATISTICS (RIGHT) TEST THE H_0 HYPOTHESIS (EQUAL MEDIANS) OF THE DIFFERENT CONDITIONS USING THE WILCOXON SIGNED-RANK TEST. SIGNIFICANT VALUES ($p \leq 0.05$) REJECTING H_0 ARE PRINTED IN BOLD.

		Descriptive Statistics						Inferential Statistics		
Metrics\Conditions		1 DoF (493)	2 DoF (493)	Horizontal (555)	Vertical (555)	Large (556)	Small (556)	1 DoF = 2 DoF	Horizontal = Vertical	Large = Small
trial time [s]	Q_2	5.68	6.88	7.06	6.14	8.22	5.60	w = 43620	w = 62291	w = 32307.5
	Q_1	3.34	4.02	4.11	3.47	4.28	3.29	**p < 0.001**	**p < 0.001**	**p < 0.001**
	Q_3	9.72	11.74	11.51	10.75	13.90	8.75			
absolute average	Q_2	$0.92 \cdot 10^{-2}$	$1.49 \cdot 10^{-2}$	$1.25 \cdot 10^{-2}$	$1.27 \cdot 10^{-2}$	$1.63 \cdot 10^{-2}$	$0.98 \cdot 10^{-2}$	w = 34089	w = 75851	w = 71071.5
size error [-]	Q_1	$0.45 \cdot 10^{-2}$	$0.91 \cdot 10^{-2}$	$0.74 \cdot 10^{-2}$	$0.68 \cdot 10^{-2}$	$0.94 \cdot 10^{-2}$	$0.53 \cdot 10^{-2}$	**p < 0.001**	p = 0.73	**p < 0.001**
[0.14 - 0.33] [2]	Q_3	$1.65 \cdot 10^{-2}$	$2.26 \cdot 10^{-2}$	$2.16 \cdot 10^{-2}$	$2.00 \cdot 10^{-2}$	$2.55 \cdot 10^{-2}$	$1.59 \cdot 10^{-2}$			
relative average	Q_2	97.21	93.70	95.22	95.57	95.56	95.22	w = 18487	w = 70566	w = 32504
size accuracy [%] [1]	Q_1	98.65	95.91	97.48	97.67	97.50	97.72	**p < 0.001**	p = 0.14	p = 0.11
[0-100] [3]	Q_3	94.99	90.06	92.29	92.86	92.75	92.15			
orientation	Q_2	6.65	17.41	14.79	10.87	11.45	12.92	w = 15658	w = 54113	w = 66391
error [deg]	Q_1	2.98	10.83	6.56	5.20	5.71	5.84	**p < 0.001**	**p < 0.001**	**p = 0.004**
[0-90] [3]	Q_3	14.13	26.09	23.87	18.26	20.34	21.96			

[1] Different than the other metrics, high scores correspond with high performance.
[2] Presents the minimal and maximal average size of the reference ellipsoids.
[3] Presents the range of the minimal and maximal scores.

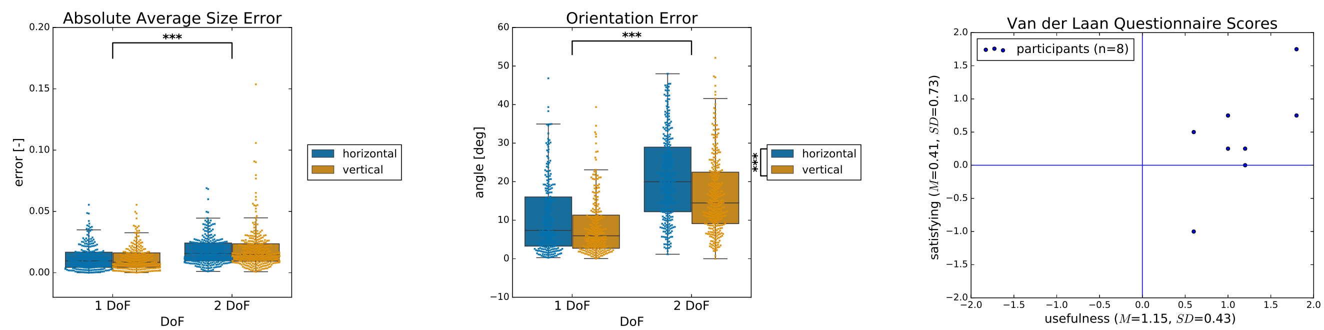

(a) (b) (c)

Fig. 5. Quantitative (a),(b) and subjective (c) results. The main metrics (a) Average shape error and (b) absolute angle are compared for the commanded DoF and Plane, where significance is denoted by: $*\ p \leq 0.05$, $**\ p \leq 0.01$, $***\ p \leq 0.001$. (c) Presents the van der Laan acceptance scores [30] that evaluate the stiffness commanding method. The horizontal axis represents the usefulness scale and the vertical axis represents the satisfying scale where the self-reported scores range from -2 (negative) to 2 (positive).

A. Performance

Comparing 1 DoF commands with 2 DoF commands, Table I, Fig. 5a and Fig. 5b show that all metrics are significant with $p < 0.001$. As hypothesized, all median values show higher performance scores in 1 DoF compared to 2 DoF, confirming the first hypothesis.

Secondly, it is hypothesized that performance in the horizontal plane is lower compared to the performance in the vertical plane for all the performance metrics. As indicated in the legend from Fig. 5a and Fig. 5b only a statistical difference is observed for the orientation error $p < 0.001$. Furthermore, Table I reveals that the absolute and relative average size error $p = 0.73$, $p = 0.14$, are not statistically significant. Therefore, the performance in the horizontal plane is lower compared to the performance in the vertical plane because it took the operator less time to command an ellipsoid (trial time $p < 0.001$); and the commanded ellipsoids are less similar to their reference ellipsoid. Where the error in similarity is based on the error in orientation $p < 0.001$ and not in the size of the stiffness commands.

Finally, it is hypothesized that the performance for large shapes is lower than small shapes for the trial time only. Table I confirms this with $p < 0.001$, however the orientation error $p = 0.004$ and absolute average size error $p < 0.001$ also show a statistical significant difference. The median values of large shapes reveal a (small) increase in performance score in orientation error but lower performance score in the absolute average size error.

B. User acceptance

In Fig. 5c the van der Laan acceptance scores are presented. All 8 participants reported a positive experience in terms of the usefulness of the stiffness commanding method. However, not all participants were satisfied with the stiffness commanding interface. Out of the 8 participants, 6 participants reported a positive score, 1 neutral and 1 participant was not satisfied. Comments during the experiment and feedback from the questions as described in (III-C) indicate that force feedback was either helpful or tiring. All participants perceived the 2 DoF commands as most difficult were 6 reported the horizontal plane as most difficult. Additionally, ellipsoids that are oriented diagonally between two axes with a 45 or 135 degree rotation were considered more difficult. Finally, comments were made on the visualizations were the orientation of small ellipsoids were difficult to see.

V. Discussion

A. System design

The perturbation signal described in (1) uses the actual position of the manipulator as a reference point. However, when integrated with an impedance controller, the choice can be made to find the interaction signal with respect to the equilibrium trajectory instead. The advantage would be that the method would not suffer from accidental stiffness decrease. The actual end-effector recordings contain high-frequency noise in the signal which is inherited in the perturbation signal. Therefore, the standard deviation of the covariance matrix is increased leading to a decrease in stiffness. On the other hand, when using the equilibrium trajectory as a reference, clear visualization of the equilibrium point is required. The operator should know with respect to what point he moves the virtual marker in order to reliably create the perturbation signal.

Furthermore, by utilizing the frequencies of the perturbation signal, the method could be further improved. If the perturbation signal is found with respect to the actual robot end-effector position, accidental stiffness decrease could be mitigated by filtering high-frequency noise from the perturbation signal. Low frequencies of the perturbation signal could also be filtered. This allows the operator to slowly move the stylus feeling the current impedance setting without decreasing the stiffness [26].

Moreover, the range between the high and low-frequency limits could be inversely related to the length of the sliding window L. If the frequency of the perturbation signal increases, the window length is decreased resulting in a higher rate of change of stiffness. As a result, the operator could provide quick perturbations (wiggles) in order to change the stiffness signal quickly, or command slow perturbations to make smaller and precise stiffens adjustments. However, increasing the rate of change of stiffness also requires more consistent and precise commands since every small change in the perturbation signal quickly changes the stiffness.

The operator receives visual feedback both from the task (through the camera's) and from the stiffness commands (through the compliance ellipsoid visualization). The virtual stiffness force feedback on the other hand only provides explicit feedback from the stiffness commands. In [25], it is stated that it is important to make the impedance observable through a haptic display since this is the way humans naturally evaluate stiffness. Different than [25], a task demonstration using the proposed method presents a visualization of the compliance ellipsoid to the operator. The visualization of the compliance ellipsoid might already provide a sufficient understanding of the stiffness commands.

In that case, the force feedback can be redesigned to incorporate both task and stiffness feedback. The haptic feedback of the stiffness commands can be designed to be more implicit while haptic feedback of the task (e.g. manipulator-environment contact) can be made explicit. Similarly to [23], the stiffness commands can be made observable by providing a back drivable force when moving the stylus. This force is not pulling the stylus back to the equilibrium position but provides a sense of inertial force while moving. If the stiffness is high, the force needed to move the stylus can be increased while low impedance results in decreased forces. Therefore, if the impedance is high the operator has to move the stylus with more effort (providing a more sluggish feeling) while low impedance allows for light and easy motion. In addition, if the robot is in contact with the environment, the force in that direction can be increased providing a sense of manipulator-environment contact. Therefore the force as an effect of the impedance can be felt during the task what could increase the remote awareness and task performance. Designing the force feedback in this way allows having feedback from both the task (explicit) and stiffness commands (implicit). The explicit task feedback might improve task performance for in-contact tasks while the implicit impedance feedback would still allow feeling the impedance during free-air movements.

B. User experiment

An experiment was set up to evaluate how well the operator is able to command stiffness variations and how the performance is influenced by different conditions.

The trial time is an indicator of overall performance for the plane and DoF conditions since it shows how quickly the participant reached satisfactory performance. It should be noted that if a subsequent trial features a differently oriented compliance ellipsoid, it took 2 seconds to rotate the compliance ellipsoid in the correct direction. Two seconds was the time needed for the temporal sliding window to have an all-new perturbation signal. The remaining time, was the time needed for the operator to improve upon their commands.

The other metrics (orientation and size error), are used to describe the similarity between the user commanded and reference ellipsoid where the performance on stiffness commands is most often a combined result of an orientation and size error. Since the 3D ellipsoid is projected on a 2D screen, the projection could show that the commanded ellipsoid matches the reference while it actually does not because of a combined size and orientation error. This error can only be spotted when looking at both the vertical and horizontal views.

Furthermore, the average size error is mostly due to the size error in the commanded direction. As an example, Table I, 1 DoF condition shows an average size error $Q_2 = 0.92 \cdot 10^2$. Therefore, the size error of the long axis would report $\approx 2.76 \cdot 10^2$ while the other two axes will have an error of ≈ 0.

As hypothesized, the results show that all performance metrics have significantly higher scores in 1 DoF commands compared to 2 DoF. In 2 DoF ellipsoids, the operator has to independently control the magnitude of 2 axes while the single DoF ellipsoid requires controlling one axis. Moreover, rotation of a single DoF ellipsoid around the long axis does not influence the stiffness matrix while a rotation around the long axis of a 2 DoF does. It is likely that those two effects increase the task complexity and therefore decrease the task performance.

Furthermore, all participants agreed that 2 DoF commands are perceived as more difficult where additional participant feedback suggests that controlling the pitch in 2 DoF was especially difficult. In theory, the interface also allows simultaneous commanding in 3 DoF. Following the trend, increasing the DoF would even further decrease the performance and is expected to be too difficult. Therefore, multiple demonstrations are necessary in order to modulate the stiffness in 3 DoF independently.

The second hypothesis expects a decrease in performance for horizontal commands compared to vertical commands. This hypothesis is partly satisfied since the overall performance indeed does decrease. The metrics trial time and orientation error show a significant decrease in performance while the relative and absolute size error does not. A potential reason could be that horizontal commands require the operator to mainly focus on the top-down view of the simulation scene. Therefore, the reference frame of the operator view, robot reference frame, and input device are not aligned leading to decreased performance.

However, this is likely not the only effect that contributes to a difference in orientation error. The kinematic structure of the human arm position allows easier movements in certain directions while more resistant to perturbation forces in other directions. Moreover, [38] and [39] revealed a significant and consistent anisotropy in force magnitude perception in the three dimensional axes. Therefore, different perceptions of force (or even movement) could contribute to a difference in performance in the horizontal and vertical planes. This is even more likely since the feedback of the participants reported to have more difficulties in orienting their stiffness commands along the diagonals ($45, 135\ deg$ rotation) within the horizontal or vertical plane condition.

It can be concluded that the commanded direction and/or reference view of the operator influences the performance of the stiffness commands through the eigenvectors only. Therefore, the viewpoint of the human, direction of the stiffness commands, and alignment with the robot reference frame should be carefully considered when maximizing performance for a task demonstration. Future work could try to distinguish what effects contribute the most to further improve the interface.

Finally, it is hypothesized that trial times for large ellipsoids are higher than small ellipsoids which are confirmed in the results. Commands that require larger movements take naturally more time compared to small movements. However, another effect is expected to contribute to the increased trial times. User feedback reports that the difference between the commanded ellipsoid and reference ellipsoid was difficult to see for small sizes. Therefore, participants could spend more time on correcting their orientation and size error for large ellipsoid since they were more aware of these errors. This is in accordance with the small significant decrease in orientation error for large sizes, which suggests that participants are able to improve performance on orientation when allowed more time.

Furthermore, the results show that the error in absolute size is significantly greater for large shapes while the relative size error is not. Large sizes result in a larger absolute over and undershoot but are in proportion to the size of the reference ellipsoid.

The van der Laan acceptance score indicates that the method is perceived as useful and intuitive. However, not everybody was satisfied. Participant feedback clarifies that participants either liked or disliked the force feedback. Additionally, some participants reported that the force feedback becomes tiring after a while. Depending on the participant, the experiment time ranged between 45 and 75 minutes. Since the method is intended for learning impedance behavior, it is unlikely that stiffness will be commanded for such long periods.

To increase user satisfaction, the most simple solution would be to lower the force feedback to prevent the operators from getting tired. Moreover, an effort could be made to improve the visual feedback complementing the force feedback. For example, force arrows on the virtual marker could point in the direction of the force where the size is represented by the magnitude. This allows the operator to have a better understanding of the system (forces). Another option could be to redesign the force feedback (as described earlier) to provide implicit haptic feedback from the stiffness commands.

C. *Comparison with other methods*

To enable learning of task appropriate impedance behavior for remote (care) robots, this study proposes a novel teleoperated stiffness commanding method. The method allows for complete modulation of the stiffness matrix in 3 DoF while being able to provide commands in 1 and 2 DoF simultaneously. The single DoF interfaces [10], [22] and [23] only allows modulation of stiffness through a specified structure (eigenvectors) of the stiffness matrix while only the magnitude (eigenvalues) of one or multiple axes can be regulated at the same time. Therefore, independent modulation of stiffness along multiple axes is not possible.

Since the proposed method provides the benefit of easily switching between orientations and magnitudes in 3 DoF, the method is best suited for tasks that consist of multiple stages. For instance, opening a microwave (Fig. II-E) consists of the approaching phase and opening phase which require 2 distinct stiffness ellipsoids. The task also shows that 1 and 2 DoF commands can be provided. Moreover, the stiffness matrix can be fixed with respect to the end-effector while the motion continues. This is especially useful when providing the more difficult 2 DoF commands.

Tele-impedance [16] also provides setting the impedance in multiple DoF. However, the operator has no conscious control in regulating the impedance. Only through co-contraction, the stiffness can be increased uniformly. Moreover, in bilateral tele-impedance setups, [40] shows that unexpected force feedback negatively impacts task performance for force-tracking tasks. Unexpected force feedback triggered human reflexes that involuntarily changed the commanded stiffness away from the desired reference stiffness.

The proposed method on the other hand, does allow conscious and full flexibility in commanding task appropriate stiffness. This however does assumes that the operator is capable of determining (and demonstrating) an appropriate stiffness profile. It is therefore not likely that even experts are able to demonstrate near-optimal stiffness variations. Task that requires near-optimal stiffness, are better of using reinforcement learning (RL) techniques [9]. However, the proposed method can be used in combination with these RL techniques. By providing a base stiffness level, RL methods might be able to converge quicker to a near-optimal stiffness profile.

In Fig. 3 the influence of the perturbation signal on the stiffness commands can be observed. From this figure, it can be seen that the stiffness change, trails behind the perturbation signal. This effect can be reduced by lowering the decreasing L and increasing f_s, however, the rate of change of stiffness will always be limited. The method is, therefore, is not suited for dynamic manipulation tasks that require timing and sudden jumps in stiffness such as catching a ball [16].

However, switching between saturation levels does not have to be problematic if the task allows pausing of the manipulator motion. This is illustrated with the task demonstration in section II-E where the manipulator motion is paused upon contact with the microwave door. In addition, high-speed motion should be slowed down because of the fixed rate of change of stiffness. Moreover, the user study shows that the operator needs some time to achieve the desired stiffness levels. The results also suggest that the operator is able to improve performance when allowed more time to command. Therefore the possibility to slow down the motion could significantly increase task performance.

Another disadvantage of tele-impedance is that it requires expensive specialized equipment for measuring muscle activity [16]. The proposed method, however, efficiently uses the same haptic master device that is used for controlling the manipulator motion providing a low-cost alternative. A potential downside is that the interface can only be used to either demonstrate motion or stiffness and does not allow to demonstrate stiffness and motion at the same time. Simultaneous motion and stiffness commands provide redundancy in force control [10] allowing the operator to find different strategies to successfully interact with the environment. Therefore, tasks that require complex interactions are more easily demonstrated due to this redundancy.

On the other hand, independence of the manipulator motion does allow the system to be used in combination with an already established motion (learning) system. Both the absence of a specialized interface and the independence of manipulator motion, allow for a cheap and easy integration for practical applications.

The stiffness commands of the proposed method are not influenced by the physical constraints of the environment. The techniques [14],[15] use the variability in motion to command stiffness. The study of [10] shows that low variability in motion does not necessarily correspond to high impedance. This is especially true for tasks that are constrained by the environment (e.g. sliding a bolt through a groove [10]). Similarly, commanding stiffness by physically perturbing the robot [25], [26], prevents to the robot to be moved in the direction of the environmental constraint. The proposed method uses virtual perturbations and is therefore independent of the environment. This increases the applicability for various tasks.

Additionally, [25],[26], [14] and [15] all require physical interaction with the robot. Inaccessible environments, large robots, or other task specifics all limit the applicability of these approaches. The proposed method is teleoperated and thus not limited to these robot and environment constraints. Therefore, the proposed method is appropriate for various domains such as space or nuclear applications, not limited to the semi-autonomous care robot.

VI. CONCLUSION

To enable learning of task appropriate impedance behavior for remote (care) robots, this study proposes a novel teleoperated stiffness commanding method. The stylus of the haptic master device is used to move a virtual marker around the end effector of the remote robot. The stiffness is determined by the amplitude of the continuous movements, where an increase in amplitude, decreases the stiffness. The method works online and the operator receives direct visual and force feedback from the stiffness commands. The interface can be used to demonstrate a base stiffness profile in simulation before the autonomous task execution. Additionally, it can be used to command stiffness during the trajectory execution.

The user study was set up to evaluate how well the operator can command stiffness variations and how the performance is influenced by different conditions. Experimental results show that 1 DoF commands perform significantly better than 2 DoF commands, and commands in the vertical plane perform significantly better than commands in the horizontal plane. The most notable result indicates that the commanded direction and/or reference view of the operator influences the performance of the stiffness commands through the eigenvectors only. Therefore, the viewpoint and pose of the human, direction of the stiffness commands, and alignment with the robot reference frame should be carefully considered to improve the stiffness commands. User acceptance is evaluated and suggests that the interface is intuitive and useful. However, user satisfaction can be increased by reducing haptic feedback or complementing this with appropriate visual feedback.

To help deciding which method is favored for what type of tasks, a general guideline is described below. Instruction (operator) based interfaces are not suited for tasks that require near-optimal stiffness profiles, are highly dynamic, or are time-critical. Therefore, RL methods are favored [9]. However, if precise tracking of position is required, bilateral tele-impedance does allow stiffness commands for dynamic task [40] as this benefits from the unconscious human reflexes.

When the environment or precise task is unknown, conscious stiffness commanding setups are favored since they allow the specification of task appropriate stiffness. The methods [10],[26], and the proposed method are all suited and each has specific benefits.

The method [10] allows for commanding of rotational stiffness. Additionally, it probably allows for an easier demonstration of contact tasks because of the redundancy in force control. However, this comes at the cost of limited flexibility in stiffness commands in 1 DoF for a predefined structure of the stiffness matrix. On the other hand, the proposed method and [26] allow for complete modulation of the stiffness matrix in 3 DoF. Therefore, integral tasks consisting of multiple stages are more easily demonstrated. In addition, these interfaces do not require complex or expensive equipment and can be used in combination with established motion systems. Finally, if the environment or robot does not allow physical interaction, [26] can not be used.

It can be concluded that the proposed stiffness commanding method is a promising approach for providing teleoperated stiffness commands. To validate the feasibility of the method, future work could investigate the task performance for a real-world manipulation task with an impedance controller. By comparing the proposed method to the current state-or-the-art stiffness commanding methods a better understanding of the performance and acceptance with respect to the other methods can be obtained. Apart from the discussed improvements on the stiffness commands, visual feedback, and haptic feedback; iterative learning of stiffness would benefit the method the most. The stiffness can be learned as function from the manipulator position such that subsequent demonstrations allow for local refinements of the stiffness matrix. Additionally, upon selection by the operator, the wiggling motion in one direction can be tied to a single rotational part of the stiffness matrix. Therefore, the operator can command the full stiffness matrix using multiple demonstrations. Similarly, this can be used to command joint stiffness for the individual joints of the manipulator.

References

[1] E. Commission, *The 2018 ageing report: Economic and budgetary projections for the eu member states (2016–2070)*, 2018.

[2] J. R. Beard, A. Officer, I. A. de Carvalho, R. Sadana, A. M. Pot, J.-P. Michel, P. Lloyd-Sherlock, J. E. Epping-Jordan, G. G. Peeters, W. R. Mahanani, *et al.*, "The world report on ageing and health: A policy framework for healthy ageing," *The Lancet*, vol. 387, no. 10033, pp. 2145–2154, 2016.

[3] D. E. Bloom, A. Boersch-Supan, P. McGee, A. Seike, *et al.*, "Population aging: Facts, challenges, and responses," *Benefits and compensation International*, vol. 41, no. 1, p. 22, 2011.

[4] T. B. Sheridan, "Telerobotics," *Automatica*, vol. 25, no. 4, pp. 487–507, 1989.

[5] B. Siciliano and O. Khatib, "Springer handbook of robotics," in. Springer, 2016, ch. Force Control, pp. 195–218.

[6] N. Hogan, "Impedance control: An approach to manipulation," in *1984 American control conference*, IEEE, 1984, pp. 304–313.

[7] P. Song, Y. Yu, and X. Zhang, "A tutorial survey and comparison of impedance control on robotic manipulation," *Robotica*, vol. 37, no. 5, pp. 801–836, 2019. DOI: 10.1017/S0263574718001339.

[8] V. Villani, F. Pini, F. Leali, C. Secchi, and C. Fantuzzi, "Survey on human-robot interaction for robot programming in industrial applications," *IFAC-PapersOnLine*, vol. 51, no. 11, pp. 66–71, 2018.

[9] J. Buchli, F. Stulp, E. Theodorou, and S. Schaal, "Learning variable impedance control," *The International Journal of Robotics Research*, vol. 30, no. 7, pp. 820–833, 2011.

[10] L. Peternel, T. Petrič, and J. Babič, "Robotic assembly solution by human-in-the-loop teaching method based on real-time stiffness modulation," *Autonomous Robots*, vol. 42, no. 1, pp. 1–17, 2018.

[11] B. D. Argall, S. Chernova, M. Veloso, and B. Browning, "A survey of robot learning from demonstration," *Robotics and autonomous systems*, vol. 57, no. 5, pp. 469–483, 2009.

[12] A. Billard, S. Calinon, R. Dillmann, and S. Schaal, "Survey: Robot programming by demonstration," *Handbook of robotics*, vol. 59, no. BOOK_CHAP, 2008.

[13] A. Pervez, A. Ali, J.-H. Ryu, and D. Lee, "Novel learning from demonstration approach for repetitive teleoperation tasks," in *2017 IEEE World Haptics Conference (WHC)*, IEEE, 2017, pp. 60–65.

[14] S. Calinon, I. Sardellitti, and D. G. Caldwell, "Learning-based control strategy for safe human-robot interaction exploiting task and robot redundancies," in *2010 IEEE/RSJ International Conference on Intelligent Robots and Systems*, Citeseer, 2010, pp. 249–254.

[15] P. Kormushev, S. Calinon, and D. G. Caldwell, "Imitation learning of positional and force skills demonstrated via kinesthetic teaching and haptic input," *Advanced Robotics*, vol. 25, no. 5, pp. 581–603, 2011.

[16] A. Ajoudani, N. Tsagarakis, and A. Bicchi, "Tele-impedance: Teleoperation with impedance regulation using a body–machine interface," *The International Journal of Robotics Research*, vol. 31, no. 13, pp. 1642–1656, 2012.

[17] C. Yang, P. Liang, Z. Li, A. Ajoudani, C.-Y. Su, and A. Bicchi, "Teaching by demonstration on dual-arm robot using variable stiffness transferring," in *2015 IEEE International Conference on Robotics and Biomimetics (ROBIO)*, IEEE, 2015, pp. 1202–1208.

[18] C. Yang, C. Zeng, P. Liang, Z. Li, R. Li, and C.-Y. Su, "Interface design of a physical human–robot interaction system for human impedance adaptive skill transfer," *IEEE Transactions on Automation Science and Engineering*, vol. 15, no. 1, pp. 329–340, 2017.

[19] M. Laghi, A. Ajoudani, M. Catalano, and A. Bicchi, "Tele-impedance with force feedback under communication time delay," in *2017 IEEE/RSJ International Conference on Intelligent Robots and Systems (IROS)*, IEEE, 2017, pp. 2564–2571.

[20] C. Yang, C. Zeng, C. Fang, W. He, and Z. Li, "A dmps-based framework for robot learning and generalization of humanlike variable impedance skills," *IEEE/ASME Transactions on Mechatronics*, vol. 23, no. 3, pp. 1193–1203, 2018.

[21] C. Yang, C. Zeng, Y. Cong, N. Wang, and M. Wang, "A learning framework of adaptive manipulative skills from human to robot," *IEEE Transactions on Industrial Informatics*, vol. 15, no. 2, pp. 1153–1161, 2019.

[22] L. Peternel, T. Petrič, E. Oztop, and J. Babič, "Teaching robots to cooperate with humans in dynamic manipulation tasks based on multi-modal human-in-the-loop approach," *Autonomous robots*, vol. 36, no. 1-2, pp. 123–136, 2014.

[23] D. S. Walker, R. P. Wilson, and G. Niemeyer, "User-controlled variable impedance teleoperation," in *2010 IEEE International Conference on Robotics and Automation*, IEEE, 2010, pp. 5352–5357.

[24] K. J. Kuchenbecker, J. G. Park, and G. Niemeyer, "Characterizing the human wrist for improved haptic interaction," in *ASME 2003 International Mechanical Engineering Congress and Exposition*, American Society of Mechanical Engineers, 2003, pp. 591–598.

[25] K. Kronander and A. Billard, "Online learning of varying stiffness through physical human-robot interaction," in *2012 IEEE International Conference on Robotics and Automation*, Ieee, 2012, pp. 1842–1849.

[26] ——, "Learning compliant manipulation through kinesthetic and tactile human-robot interaction," *IEEE transactions on haptics*, vol. 7, no. 3, pp. 367–380, 2014.

[27] A. Ajoudani, N. Tsagarakis, and A. Bicchi, "Tele-impedance: Teleoperation with impedance regulation using a body–machine interface," *The International Journal of Robotics Research*, vol. 31, no. 13, pp. 1642–1656, 2012.

[28] V. Ho, C. Borst, M. M. van Paassen, and M. Mulder, "Increasing acceptance of haptic feedback in uav teleoperation by visualizing force fields," in *2018 IEEE International Conference on Systems, Man, and Cybernetics (SMC)*, IEEE, 2018, pp. 3027–3032.

[29] W. Vreugdenhil, "Complementing automotive haptic shared control with visual feedback for obstacle avoidance," 2019.

[30] J. D. Van Der Laan, A. Heino, and D. De Waard, "A simple procedure for the assessment of acceptance of advanced transport telematics," *Transportation Research Part C: Emerging Technologies*, vol. 5, no. 1, pp. 1–10, 1997.

[31] R. E. Wood, "Task complexity: Definition of the construct," *Organizational behavior and human decision processes*, vol. 37, no. 1, pp. 60–82, 1986.

[32] B. P. DeJong, J. E. Colgate, and M. A. Peshkin, "Improving teleoperation: Reducing mental rotations and translations," in *IEEE International Conference on Robotics and Automation, 2004. Proceedings. ICRA'04. 2004*, IEEE, vol. 4, 2004, pp. 3708–3714.

[33] D. Q. Huynh, "Metrics for 3d rotations: Comparison and analysis," *Journal of Mathematical Imaging and Vision*, vol. 35, no. 2, pp. 155–164, 2009.

[34] S. S. Shapiro and M. B. Wilk, "An analysis of variance test for normality (complete samples)," *Biometrika*, vol. 52, no. 3/4, pp. 591–611, 1965.

[35] M. A. Stephens, "Tests of fit for the logistic distribution based on the empirical distribution function," *Biometrika*, vol. 66, no. 3, pp. 591–595, 1979.

[36] ——, "Goodness of fit for the extreme value distribution," *Biometrika*, vol. 64, no. 3, pp. 583–588, 1977.

[37] F. Wilcoxon, "Individual comparisons by ranking methods," in *Breakthroughs in statistics*, Springer, 1992, pp. 196–202.

[38] F. E. van Beek, W. M. B. Tiest, and A. M. Kappers, "Anisotropy in the haptic perception of force direction and magnitude," *IEEE transactions on haptics*, vol. 6, no. 4, pp. 399–407, 2013.

[39] F. E. Van Beek, W. M. B. Tiest, W. Mugge, and A. M. Kappers, "Haptic perception of force magnitude and its relation to postural arm dynamics in 3d," *Scientific reports*, vol. 5, no. 1, pp. 1–11, 2015.

[40] L. M. Doornebosch, D. A. Abbink, and L. Peternel, "The force-feedback coupling effect in bilateral tele-impedance," in *2020 8th IEEE RAS/EMBS International Conference for Biomedical Robotics and Biomechatronics (BioRob)*, IEEE, pp. 152–157.

A

System Implementation

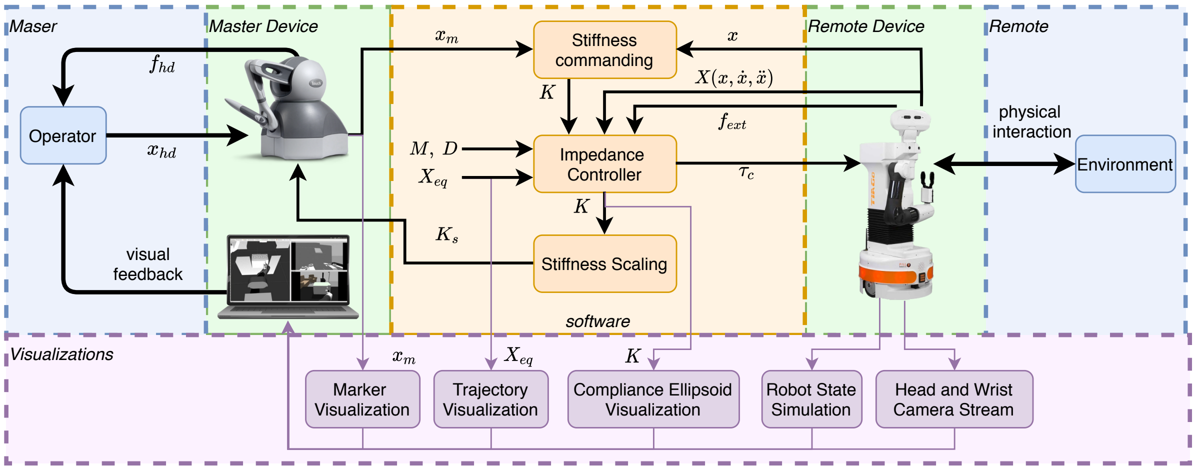

Figure A.1: System overview containing the most important software blocks, signals and apparatus. The operator and the remote environment (blue sections) interact with the master and remote devices respectively (green sections). The yellow section contains the software blocks and signals and the purple section shows the visualization based on the important signals or robot sensors.

A.1. Hardware setup

The telemanipulation setup consisted on the master side of a laptop with a computer screen and a Geomagic Touch [1]. The master side uses the Geomagic Touch that allows for 6 DoF pose (position + orientation) inputs and 3 DoF transitional haptic feedback. In addition, the laptop uses Ubuntu 16.04 in combination with ROS-Kinetic.

The 'remote' side featured the simulation of a prototype of the Tiago Robot [2] named Marco. The Marco simulation is provided through a Unified Robot Description Format (urdf) containing all the kinematic, dynamic, sensor, and transmission (controller) properties. This information is provided by PAL robotics and is tuned to be as similar as possible as the actual robot hardware. Therefore, the simulation and the real robot are interchangeable and require minimal adjustments when switching from the simulation to the actual robot.

A.2. Software

The software runs in Ubuntu 16.04 using ROS-Kinetic (Robotic Operating System). The workspace ***omni_marco_gazebo*** is initialized using existing packages necessary to run the Marco simulation. The repository can be found here:
https://github.com/JLSchol/omni_marco_gazebo/tree/devel_graduation_package.

The following subsections describe the important parts of the workspace and thesis implementation. Every subsection contains a list of the created packages with a small description of their content.

A.2.1. Haptic Device

The following package is created to run the haptic device (omni/ Geomagic Touch) in combination with the stiffness commanding packages. These packages require the old drivers of the Geomagic Touch of 2016 when used in combination with ubuntu 16.04 and ROS-Kinetic.

- **phantom_omni –** This package contains the file that allows communication between the Geomagic Touch and the system running ROS. It initializes and calibrates the Geomagic Touch. Furthermore, it publishes the joint states, button events, and cartesian position while it allows subscribing to (setting of) force feedback topics.
- **haptic_device_rotation –** This package allows adding the frame definition of the omni to any reference frame of the robot. It requires the use of TF [3] that tracks the frames of the robot in ROS. It requires setting the rotation matrix describing the mapping of the Omni (child) frame to a robot (parent) frame.
- **omni_description –** Package containing the urdf model of the omni.

A.2.2. Stiffness Commanding Implementation

- **stiffness_launch –** Contains three launch files.
  - file that launches the omni + stiffness pkgs + marco in simulation.
  - file that launches Omni + stiffness pkgs + a fake end effector (used for the user experiment)
  - file that launches only the Omni + stiffness pkgs. This allows us to launch Marco in a gazebo environment separately. Used in combination with the task demonstration.
- **haptic_device_2_marker –** Package publishing a virtual marker representing the stylus movements of the Omni. The scaled marker moves around the end-effector of the robot manipulator.
- **stiffness_commanding –** Package that converts the Omni stylus movements to stiffness commands. It publishes the covariance matrix; eigenvalues and vectors of the covariance matrix; the stiffness matrix and the eigenvalues and vectors of the stiffness matrix. It requires setting minimal and maximal stylus deviation limits, the minimal and maximal manipulator stiffness limits, and the length of the sliding window.
- **stiffness_feedback_feedback_forces –** This package calculates the feedback forces by scaling down the manipulator stiffness. The feedback forces are then published to the **phantom_omni** pkg. It requires setting the maximal force and allowed deviation of the haptic device.
- **stiffness_visualization –** Contains the compliance ellipsoid visualization node. Additionally, it contains an ellipsoid class used for various ROS (ellipsoid)msgs conversions and helper functions relating to the stiffness commanding implementation and user experiments.
- **data_processing –** Package used to record, process and plot general data from the stiffness commanding implementation. It can be used to plot data from task demonstrations, test inputs or any other topic used in the stiffness commanding implementation. It does not process and plot the user experiment data which is done separately in **stiffness_simple_experiment**.
- **test_common –** Package that contains different base test inputs that allow running the code independently from the haptic device and robot simulation. Also used for integration testing of the nodes.

A.2.3. User Experiment

The user experiment contains a single package: **stiffness_simple_experiment**. It contains the implementation of the user experiment and additional files to record, process, analyze, and plot the experimental data. The experiment implementation contains:

- The GUI implementation is used by the researcher to run, manage, and supervise the experiment. It also allows adding notes during the experiment.

- The GUI implementation as presented to the participant to view the experiment.
- The experiment logic (implementation).

Additional files to record, process, analyse and plot :

- Bash file to record (rosbag) the experiment.
- Bash file to extract topics included in the rosbag to csv files.
- File used to create the data directories based on experiment recordings.
- Class used to store all data related to a single participant conveniently.
- File that processes the data .
- File used to plot the data.
- File used to analyze the data.

A.2.4. Task Demonstration

The task demonstration is implemented in the single **stiffness_experiment** package and includes the following:

- Node with the gazebo world (with the micro_wave).
- Node that fixed the micro_wave in the simulation world.
- Path planner used to command the end-effector of the robot.

The files can be launched in combination with the Omni + stiffness launch file located in **stiffness_launch**.

A.2.5. Impedance Controller

The implementation of the Impedance Controller was not finished see section A.4. Eventually, only controller configurations, gazebo configurations, and a part of a cartesian controller plugin were written following the ros_control framework [4]. The controller plugin contains a complete setup which can be used as a basis for an impedance controller (or any other Cartesian controller since the code that requests the inverse kinematics needed is already present). The custom controller plugin builds and loads correctly in the controller manager of the marco gazebo simulation. However, The plugin was not able to write commands to the gazebo simulation while it was able to read the commands in the file (controller plugin):

```
omni_marco_gazebo/src/custom_controllers/cart_pos_based_impedance_controller/src/CartPBImpedanceController.cpp
```

The line `joints_[i].getPosition();` does work while the line `joints_[i].setCommand(commanded_position);` does not. The following pkgs are created:

- **custom_controllers/cart_pos_based_impedance_controller –** Contains the controller plugin.
- **marco_controller_configuration_gazebo –** contains the controller configuration files.

A.3. Software testing and evaluation

Different modules of the software (stiffness commands, force feedback) are tested using integration tests. In the package **test_common**, different test inputs are created and used as inputs for the individual modules. These tests are also used to vary the controlled input and investigate the effects on different parameters of the software. These inputs are also used to test the system as a whole without being dependent on the robot and haptic device. After the controlled inputs, human inputs are provided to the system and visually inspected.

A.4. Impedance controller

Initially, the idea was to implement an impedance controller on Marco. However, this implementation was stopped since the desired impedance implementation scheme produces torque commands Fig. A.2b. Therefore, it requires a torque-controlled manipulator. The joints of Marco are position controlled but allow torque commands through an effort interface for the first 4 joints with a limited rate of 50 Hz. The remaining 3 joints would require defining an 'admittance' to map the joint torques to position commands. Both the limited rate for the first four joints and defining an admittance could cause difficulties for the implementation and could cause instabilities upon contact with stiff environments.

The other option would be to implement position-based impedance control Fig. A.2a. Sometimes also referred to as admittance control [5]. The problem of this implementation scheme is that the controller is unstable in stiff environments (see Fig. A.2d) because the inner (stiff) position control loop dominates over the outer (softening) impedance loop. Since the manipulator of the care-robot deals with stiff environments, this implementation is not suited. Therefore, the choice was made to bypass the impedance controller and directly connect stiffness commands to stiffness scaling in Fig. A.1.

Impedance control can be implemented using Joint or Cartesian space representation. Depending on the task, one representation may be favored over the other. Generally speaking, tasks that require moving or manipulating objects in Cartesian space benefit from the Cartesian space representation (e.g. opening a door). The stiffness commanding method is suited for Cartesian space representations although modifications could be made to command a single joint at the time. Furthermore, depending on the robot hardware and accurate knowledge of the dynamics and manipulator, impedance control is realized in slightly different ways. In this section, the general impedance model equation will be described. For completeness, a torque-controlled manipulator with known dynamics will be used as an example for illustrating the control objective in relation to the impedance model (Fig. A.2c).

$$\boldsymbol{f_{ext}} = \boldsymbol{M}(\ddot{\boldsymbol{x}} - \ddot{\boldsymbol{x}}_{\boldsymbol{eq}}) + \boldsymbol{D}(\dot{\boldsymbol{x}} - \dot{\boldsymbol{x}}_{\boldsymbol{eq}}) + \boldsymbol{K}(\boldsymbol{x} - \boldsymbol{x_{eq}}) \tag{A.1}$$

Here, the general impedance model equation is given where $\boldsymbol{M},\ \boldsymbol{D},\ \boldsymbol{K} \in \mathbb{R}^{\boldsymbol{6\times6}}$ denotes the desired inertia, damping and stiffness matrices, $\boldsymbol{f_{ext}} \in \mathbb{R}^{\boldsymbol{6\times1}}$ represents the contact force/torque vector on the manipulator and $\boldsymbol{x},\ \boldsymbol{x_{eq}} \in \mathbb{R}^{\boldsymbol{6\times1}}$ refer to the actual and equilibrium position vectors for translational and rotational DoF. By substituting the model equation (A.1) into the manipulator equation of motion (A.2), the commanded joint torques $\boldsymbol{\tau_c} \in \mathbb{R}^{\boldsymbol{6\times1}}$ can be controlled such that the impedance model equation (A.1) holds.

$$\boldsymbol{I}(\boldsymbol{q})\ddot{\boldsymbol{q}} + \boldsymbol{C}(\dot{\boldsymbol{q}},\boldsymbol{q})\dot{\boldsymbol{q}} + \boldsymbol{G}(\boldsymbol{q}) + \boldsymbol{f_f}(\dot{\boldsymbol{q}}) = \boldsymbol{\tau_c} - \boldsymbol{J}^{\boldsymbol{T}}\boldsymbol{f_{ext}} \tag{A.2}$$

Where $\boldsymbol{I},\boldsymbol{C}, \in \mathbb{R}^{\boldsymbol{6\times6}}$ and $\boldsymbol{f_f},\boldsymbol{G} \in \mathbb{R}^{\boldsymbol{6\times1}}$ are the manipulator Inertia, Coriolis and Centrifugal, gravity and friction components respectively. $\boldsymbol{J} \in \mathbb{R}^{\boldsymbol{6\times6}}$ is the manipulator Jacobian matrix used to map between joint and Cartesian space and $\boldsymbol{q} \in \mathbb{R}^{\boldsymbol{6\times1}}$ is a vector of the manipulator joint angles.

No assumptions are made on how the equilibrium trajectory (variables $\boldsymbol{X_{eq}} \widehat{=} (\ddot{\boldsymbol{x}}_{\boldsymbol{eq}}, \dot{\boldsymbol{x}}_{\boldsymbol{eq}}, \boldsymbol{x_{eq}})$) is obtained. Furthermore, the stiffness commanding method is not used to set the desired damping and Inertia $\boldsymbol{D},\boldsymbol{M}$. The desired Inertia is commonly set to be equal to the manipulator's Inertia matrix $\boldsymbol{I}$ while the desired Damping can either be fixed, made a function of the desired stiffness $\boldsymbol{K}$, or be related to the perturbation signal as proposed in [6].

A.5. Stiffness commands from perturbation signal

The stiffness commanding method is intended to command for the 3 translational DoF. Therefore only a sub-matrix from the complete stiffness matrix as described in (A.1) can be varied. The $\boldsymbol{6\times6}$ symmetric and positive-definite (SPD) stiffness matrix can be divided into four $\boldsymbol{3\times3}$ SPD sub-matrices.

$$\boldsymbol{K} = \begin{bmatrix} \boldsymbol{K_{fp}} & \boldsymbol{K_{fr}} \\ \boldsymbol{K_{tp}} & \boldsymbol{K_{tr}} \end{bmatrix} \tag{A.3}$$

Where only $\boldsymbol{K_{fp}}$ is set using the stiffness commanding method relating the contact forces to position errors. The sub-matrices $\boldsymbol{K_{tr}},\ \boldsymbol{K_{fr}},\ \boldsymbol{K_{tp}}$ relate: torques to rotation errors, forces to rotation errors and torques to position errors. Commanding or specification of the other matrices are not taken into account in this research. However, $\boldsymbol{K_{tr}},\ \boldsymbol{K_{fr}}$ could be set to zero and $\boldsymbol{K_{tp}}$ high to prevent rotation of the end-effector.

The stiffness matrix is found, by setting it inversely proportional to the covariance matrix. This covariance matrix is constructed based on a data matrix that contains the perturbation signals that is created by the

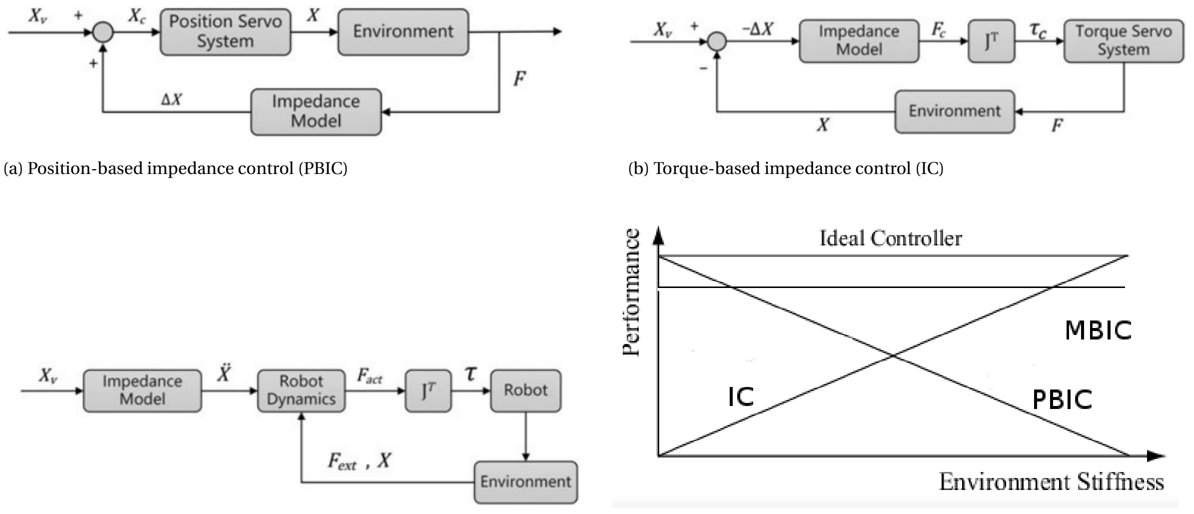

(a) Position-based impedance control (PBIC)

(b) Torque-based impedance control (IC)

(c) Model-based impedance control (MBIC)

(d) Comparison controller performance along environment stiffness.

(a)-(c) are different simplified implementation schemes of impedance control from [7]. (d) Illustrates the controller performance along the environment stiffness.

operator moving (wiggling) the stylus. The length of the data matrix is determined by the length of the sliding window. The implementation is described in the method section of the research paper 1.

First, a small MATLAB implementation is made to see if the stiffness decrease and increase would behave as expected. Next, the implementation was made in ROS and tested. By providing different input signals as stylus deviations the stiffness commanding module is evaluated. Different properties are investigated and are visualized in Fig. A.3. The following is investigated:

1. checked if the stiffness and perturbation limits behaved correctly.
2. influence on different amplitudes.
3. influence of different frequencies.
4. noise on the stiffness signal.
5. influence of the length of the sliding window.
6. 2 Dof circular inputs.

A human perturbation can be seen from Fig. A.4. In Fig. A.3a the reference perturbation signal is plotted. From this figure it can be seen that the stiffness is limited to the max (1000 $[Nm]$) and min (100 $[Nm]$) for perturbations between 0.707 $[m]$ and 0.3 $[m]$. Additionally, the covariance matrix and subsequently the stiffness is calculated over the data matrix with a length of 1 $[s]$. It can be seen that stiffness trails behind the actual perturbation signal. Finally, it can be noticed that the lower stiffness limit (around 7.2 $[s]$) is reached relatively quickly compare to the decreasing signal between $4.5 - 5.5$ $[s]$. This is due to the perturbation signal that overshoots the perturbation limits. Therefore the stiffness limit is reached before the signal would flatten if no limits were present.

In Fig. A.3b the influence of noise (sampled from normal distribution with $SD = 0.025$) on the perturbation signal is presented. Between $1 - 2$ $[s]$ it can be seen that the stiffness slightly drops below 1000 $[Nm]$ as results of this noise. This noise can be presented in the end-effector recordings of the actual position of the manipulator which can result in a slight stiffness decrease.

In Fig. A.3c the frequency is doubled with respect to Fig A.3a. This has no effect on the general slope of the rate of change of stiffness except for the fact that the in/decreasing signal has more 'bumps' and therefore will more gradually change. On the other hand, Fig. A.3d does show a lower rate of change of stiffness. This is due to doubling the length of the sliding windows. Therefore the data matrix has a length corresponding to 2 $[s]$ instead of 1 $[s]$. The covariance matrix and subsequently the stiffness is computed over a larger range of data points that decrease the rate of change.

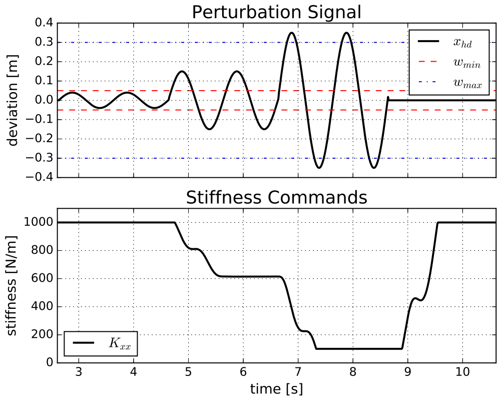

(a) Reference perturbation signal.

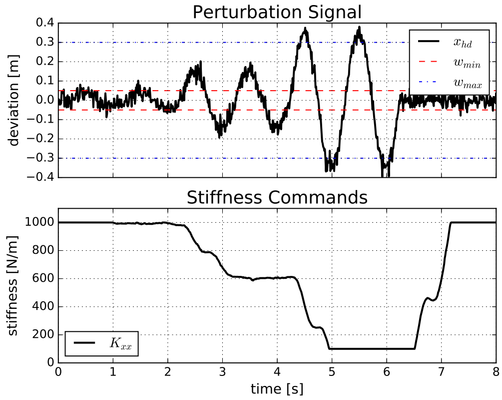

(b) Perturbation signal with noise.

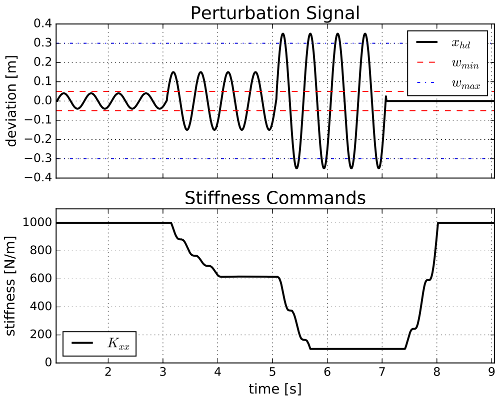

(c) Perturbation signal with doubled frequency.

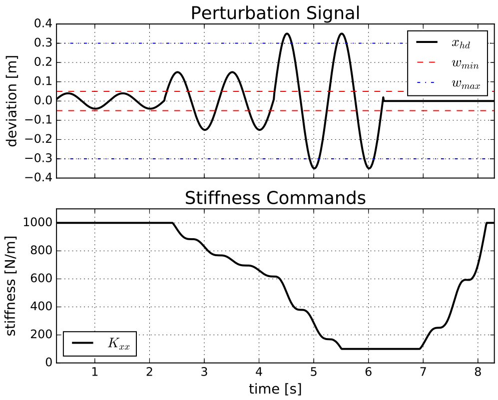

(d) Perturbation signal with doubled sliding window length.

Figure A.3: Influence of different condition on stiffness commands.

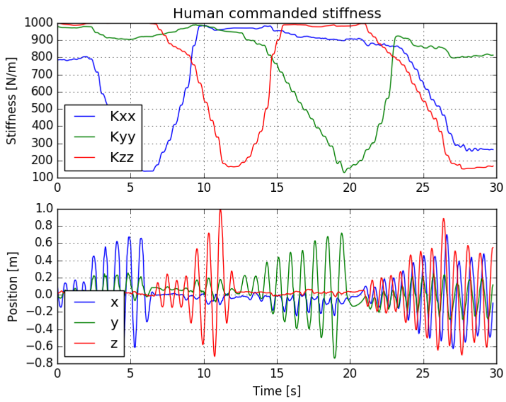

Figure A.4: Stiffness commands based on a human perturbation signal for 1 (0-20 seconds) and 2 DoF (22 - 30 seconds) commands.

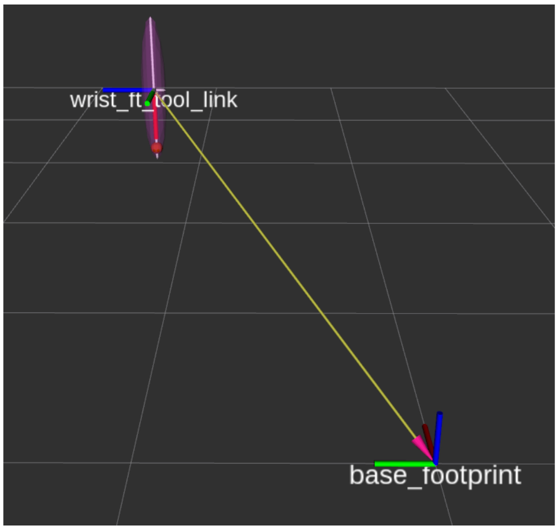

Figure A.5: Compliance ellipsoid visualization. Ellipsoids is presented in purple while the axes are presented with white arrows.

Finally, Fig. A.4 shows the stiffness based on a human perturbation signal. Perturbation is given in 1 DoF along the three principal axes until 20 s. Next 2 DoF perturbation is given by creating a circular motion between $22-30$ $[s]$.

A.5.1. Compliance ellipsoid visualization

The visualization of the compliance ellipsoid (included in package **stiffness_visualization**) is created to provide visual feedback of the stiffness commands. Because a stiffness ellipsoid is an inverse representation of the compliance ellipsoid, we can use the decomposed covariance matrix to represent the compliance ellipsoid. It is created based of the eigenvalues and eigenvectors of the covariance matrix.

$$\boldsymbol{\Sigma} = \boldsymbol{Q}\boldsymbol{\Lambda}\boldsymbol{Q}^{\boldsymbol{T}} \tag{A.4}$$

Where $\boldsymbol{\Sigma}$, $\boldsymbol{Q}$, $\boldsymbol{\Lambda}$ are the covariance matrix, eigenvectors matrix, and the diagonal matrix with eigenvalues. Next, the square root of the eigenvalues is presented by $\sigma_i = \sqrt{\lambda_i}$ which represents the standard deviation of the perturbation signal. Since the covariance matrix is a symmetric (and positive-definite) matrix, the eigenvalues and eigenvectors can be solved using a self-adjoint ($A = A^t$) solver to find the eigenvalue decomposition. The solver returns the eigenvalues and eigenvectors, however, in no specific order. Every vector is paired with a value but the order of Q and Λ is arbitrary. Therefore, the matrix Q does not necessarily present a rotation matrix in the right-handed frame convention. To find a valid rotation matrix, the determinant of the matrix should be checked. If the determinant is equal to 1, Q is associated with a rotation with a right-handed frame convention. If the determinant is equal to -1, Q is associated with a rotation in the left-handed frame convention or can represent a reflection of the axis definition in the right handed frame. If the determinant is -1, a correct orientation can be found by multiplying a single eigenvector-value pair with -1 or by shuffling any 2 eigenvector-value pairs once. This will result in Q associated with a right-handed rotation. Finally, the rotation matrix is converted to a unit quaternion.

The next step is to limit $\sigma_i = \sqrt{\lambda_i}$ such that they correspond to the maximum and minimal allowed stylus perturbations. This will also ensure a minimal and maximal representation of the compliance ellipsoid. This is simply done by checking values of σ and limit them to $\underline{\sigma}$ or $\bar{\sigma}$ when below or above the limits. The values are multiplied by 2 to represent the diameters d of the compliance ellipsoid.

$$d_i = \begin{cases} 2\underline{\sigma} & \sigma_i < \underline{\sigma} \\ 2\bar{\sigma} & \sigma_i > \bar{\sigma} \\ 2\sigma_i, & \text{otherwise} \end{cases} \tag{A.5}$$

Using the unit quaternion (based on $\mathbf{Q}$), the diameters d_i (based on Λ), and the actual end-effector position of the end-effector, the ellipsoid visualization is made. Additionally, the diameters are visualized with white arrows and both are implemented using RVIZ [8]. Note that RVIZ does not require specification of the surface points of the ellipsoid. The visualization can be seen in Fig. A.5.

A.6. Force feedback implementation

Starting with the stiffness matrix decomposition.

$$\boldsymbol{K_{fp}} = \boldsymbol{Q}\boldsymbol{\Gamma}\boldsymbol{Q}^{\boldsymbol{T}} \tag{A.6}$$

The minimal and maximal stiffness of the haptic device is defined by relating this to the maximal allowed stylus deviation and the force range.

$$\begin{aligned} \underline{K}_{hd} &= \frac{\underline{f}_{hd}}{\bar{x}_{hd}} \\ \bar{K}_{hd} &= \frac{\bar{f}_{hd}}{\bar{x}_{hd}} \end{aligned} \tag{A.7}$$

By relating the maximal and minimal manipulator stiffness ($\bar{K}_{fp}$. $\underline{K}_{fp}$) to the maximal and minimal allowed haptic device stiffness, the scaled down stiffness its eigenvalues can be found.

$$\mathbf{K_{s,e}} = \underline{\mathbf{K}}_{\mathbf{hd}} + \frac{\bar{K}_{hd} - \underline{K}_{hd}}{\bar{K}_{fp} - \underline{K}_{fp}}(\Gamma - \underline{\mathbf{K}}_{\mathbf{fp}}) \tag{A.8}$$

Next the scaled down stiffness is found by rotating back the diagonal matrix with scaled stiffness eigenvalues.

$$\mathbf{K_s} = \boldsymbol{Q}\boldsymbol{K_{s,e}}\boldsymbol{Q}^{\boldsymbol{T}} \tag{A.9}$$

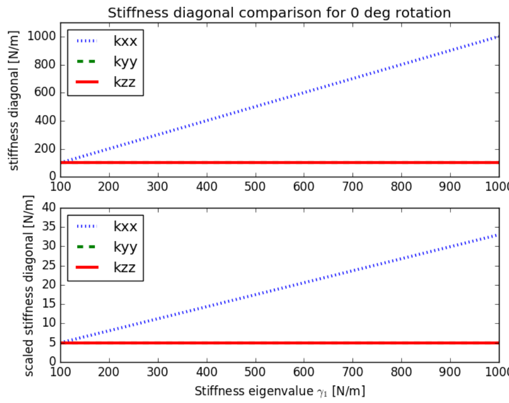

(a) Stiffness scaling for a 0 degree rotated stiffness matrix around z-axis

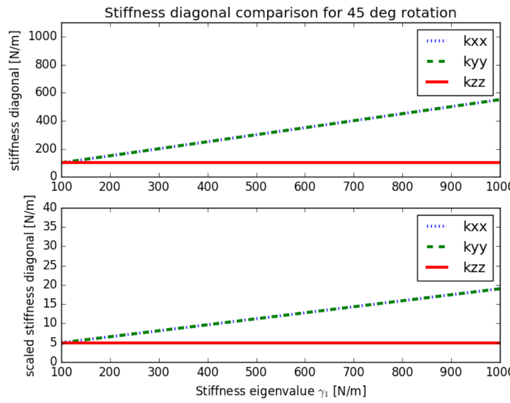

(b) Stiffness scaling for a 45 degree rotated stiffness matrix around z-axis

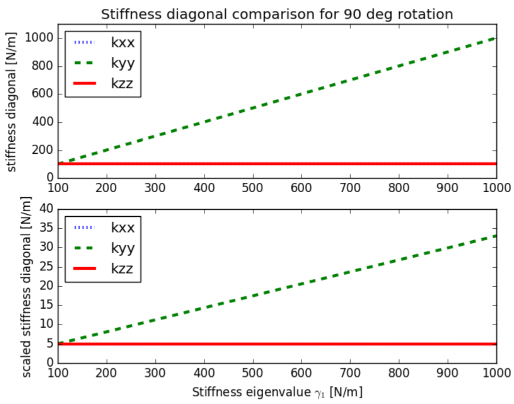

(c) Stiffness scaling for a 90 degree rotated stiffness matrix around z-axis

Figure A.6: These plots show how the manipulator stiffness matrix and the haptic device stiffness compare when a single eigenvalue of the manipulator stiffness is varied between the manipulator stiffness limits (rest is 0). The three different plots show three different orientations of the stiffness ellipsoid that is rotated around the z-axis. The manipulator stiffness limits are $100-1000$ $[Nm]$. The maximal allowed stylus deviation is $\bar{x}_{hd} = 0.1$. The minimal and the maximal allowed force for maximal stylus deviation are $\bar{f}_{hd} = 3.3$ and $\underline{f}_{hd} = 0.05$ respectively.

Where $\underline{\mathbf{K}}_{\mathbf{hd}}$, $\underline{\mathbf{K}}_{\mathbf{fp}}$ and $\bar{\mathbf{K}}_{\mathbf{fp}}$ are diagonal matrices with on the diagonals $\underline{K}_{hd}$, $\underline{K}_{fp}$, $\bar{K}_{fp}$ respectively. Subsequently, the force feedback is calculated by

$$\boldsymbol{f_{hd}} = \boldsymbol{K_s x_{hd}} \tag{A.10}$$

In Fig. A.9 the plots show that the commanded stiffness is correctly scaled. From A.6a it can be seen that by increasing a single eigenvalue from the minimal to the maximal impedance controller limit $[100-1000]$, the scaled stiffness also ranges from the minimal $5 = \frac{0.05}{0.1}$ to the maximal $33 = \frac{3.3}{0.1}$ as defined in (A.7.

Additionally, Fig A.7 shows the force as response from an input perturbation. It shows that the defined minimal and maximal defined force $[0, 3.3]$ Nm matches the force response from a minimal and maximal perturbation.

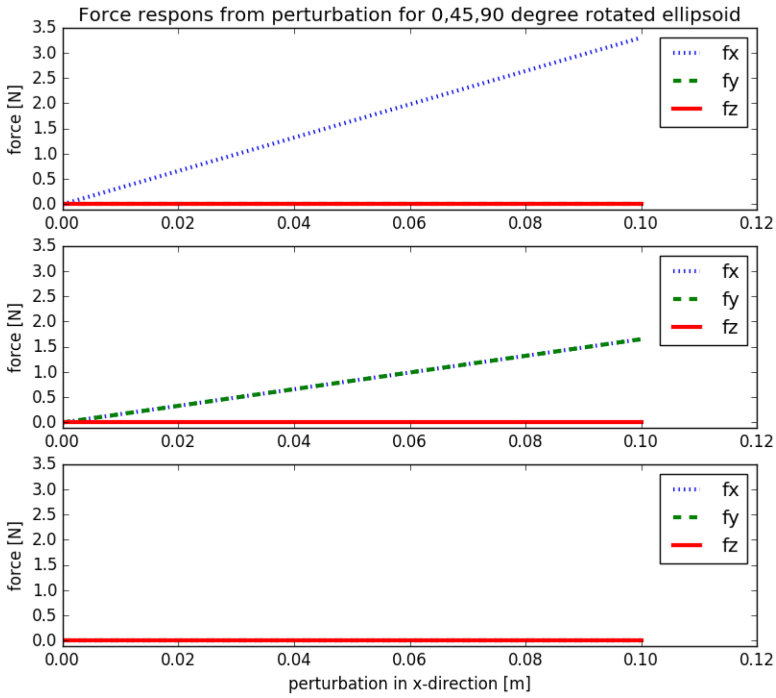

Figure A.7: Force response from a perturbation in the x-direction for a 0, 45 and 90 degree rotated stiffness ellipsoid (with eigenvalues [e1=1000, 0, 0]) over the z-axis. The minimal and the maximal allowed force for maximal stylus deviation are $\bar{f}_{hd} = 3.3$ and $f_{hd} = 0$ and the maximal stylus deviation is $\bar{x}_{hd} = 0.1$. From the top plot, it can be seen that the force is indeed limited to 3.3 Newton for maximal perturbation of 0.1 m

B

Experiment Implementation

The experiment is implemented in ROS and visualized in RVIZ. The scene that is viewed by the participant is implemented through a Graphical User interface (GUI) and described in section B.3. The experiment is managed through GUI and described in section B.2. The settings from the stiffness experiment are experimentally defined through the pilot study. The settings used for the experiment are:

Tune parameters	
virtual marker scaling	5
$[\underline{\sigma}, \bar{\sigma}]$	$[0.0424, 0.283]$
L	200
f_s	100 HZ
$[\underline{k}, \bar{k}]$	$[10, 1000]$ Nm
$[\underline{f}_{hd}, \bar{f}_{hd}]$	$[0, 2.5]$ N
$\underline{x}_{hd}$	0.05 m

In the experiment 3 types of compliance, ellipsoids were presented namely cigar, oval and circle shaped ellipsoids. All were represented in small or large sizes and in the horizontal and vertical planes. The cigar and oval-shaped ellipsoids are presented in four different orientations and the circle-shaped ellipsoid only in 1 orientation. Therefore, there are 36 distinct ellipsoids identified by their: type, plane, size, and orientation. All are repeated 4 times each totaling 144 compliance ellipsoids per experiment. The order of the ellipsoids is randomly set using a fixed seed, therefore every participant has the same random order.

type	Large (principle axis)	Small (principle axis)	Orientations [deg] in plane	Commanded DoF	Planes	Total Amount in single experiment
cigar	[0.458, 0.0849, 0.0849]	[0.251, 0.0849, 0.0849]	[0, 45, 90, 135]	1	horizontal + vertical	64
oval	[0.458, 0.229, 0.0849]	[0.251, 0.126, 0.0849]	[0, 45, 90, 135]	2	horizontal + vertical	64
circle	[0.458, 0.458, 0.0849]	[0.251, 0.251, 0.0849]	0	2	horizontal + vertical	16

Every experimental condition is launched and recorded separately. The experiment recorded using rosbag which recorded all the topics. Therefore, the experiment can be played back as a whole including the visualizations.

For each condition, a reference compliance ellipsoid has to be created that represents a stiffness matrix. The reference ellipsoid is created by specifying the diameters of the principal axis and the unit quaternion representing the rotation. The user commanded ellipsoid is created following the process described in section A.5.1. However, the user commanded ellipsoid, and reference ellipsoid can not directly be compared on size and orientation. This process is described in B.1

B.1. Comparison of user commanded and reference ellipsoid

The reference ellipsoid is spawned using 3 diameters of the principal axis and oriented using a unit quaternion. Therefore, we must find the diameters and quaternion from the commanded ellipsoid to compare.

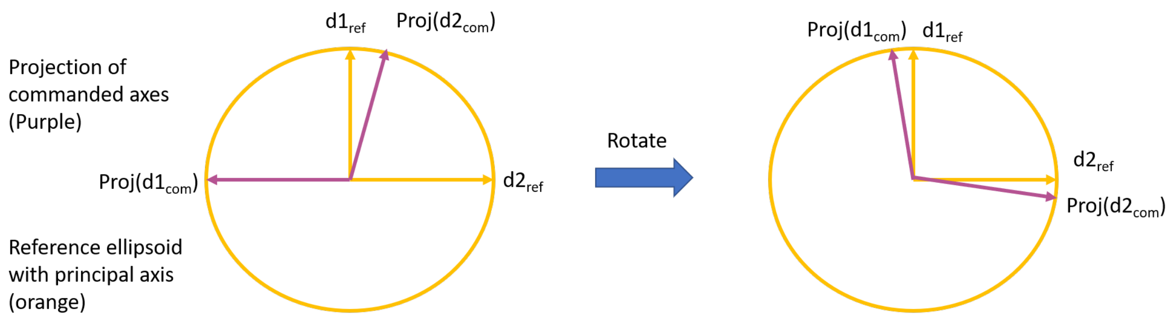

Figure B.1: Illustration of finding the closest rotation for shapes with two identical eigenvalues. Note that the projected axis is not perpendicular to each other since the third axis (not showing) of the commanded ellipsoid is most often not aligned with the third axis of the reference ellipsoid. Therefore, the rotation is the summed angle between $proj(d2_{com})$ - $d2_{ref}$ and $proj(d1_{com})$ - $d1_{ref}$ divided by two.

The orientation and diameters of the user commanded ellipsoid are based on the eigenvalues and eigenvectors from the eigendecomposition of the stiffness matrix which is described in A.5.1. This decomposition returns random indexing of the vector values pairs. From the 6 possible configurations, only 3 are correct and have a $det(R) = 1$ which is associated with a rotation with right-handed frame definition. These three combinations of vector value pairs are correctly representing the same compliance ellipsoid. However, the rotation is different for the possible combinations. For example, the vector (V) value pairs (e):

- $R_1 = [V_1, V_2, V_3],\ E_1 = [e_1, e_2, e_3]$
- $R_2 = [V_2, V_3, V_1],\ E_2 = [e_2, e_3, e_1]$
- $R_3 = [V_3, V_1, V_2],\ E_3 = [e_3, e_1, e_2]$

all correctly represent the same compliance ellipsoid however the rotation described by R_1 R_2 R_3 are not equal! Therefore, we must chose the correct representation that matches the reference ellipsoid.

Moreover, there is another problem when comparing ellipsoids. If the reference ellipsoid has two or more axis that is equal (e.g. $e_1 = e_2$ which is the case for circular or cigar-shaped ellipsoids), there are infinite rotations that describe the correct ellipsoid. If the user is commanding in 1 DoF by wiggling the stylus from left to right, a cigar-shaped compliance ellipsoid is formed with one long axis in the direction of movement. The other two axis perpendicular to the movement are equally small and represent the maximal stiffness limits. Therefore, we can have infinite rotations around the long axis which all correctly show the same compliance ellipsoid but have different orientations.

Lets denote the reference and commanded diameters and rotation with d_{ref}, R_{ref}, d_{com}, R_{com} respectively. Where the diameter d is a scaled representation of the eigenvalues E. The algorithm used to find the quaternion closest to the reference orientation is presented in algorithm 1. This algorithm is based on finding the characteristic axis. The characteristic axis is defined to be the axis that identifies the shape. This axis is used to align the characteristic axis of the user commanded ellipsoid with the characteristic axis of the reference ellipsoid. For cigar-shaped ellipsoid, this is the long principle axis, for circular shaped and oval ellipsoids this is the short axis. Next the characteristic axes of the user and reference ellipsoid are pointed in the same direction by shuffling the vector value pairs of R_{com} and d_{com} producing $R_{s,com}$ and $d_{s,com}$. If the commanded and reference ellipsoid are both oval-shaped the algorithm is finished. If either the reference or the commanded ellipsoid is cigar or circular shaped, the commanded ellipsoid has to be rotated with angle α over the characteristic axis to find the closest representation of the reference orientation. This is done by using vector projections of the commanded ellipsoid on the reference ellipsoid. The process is illustrated in Fig. B.1. It should be noted that if the commanded ellipsoid has three equal axes no orientation can be found. This is likely not to happen as this requires 3 DoF commands with exactly equal eigenvalues. The experiment only asks for 1 and 2 DoF commands.

Now the rotation and the diameters of the reference and commanded compliance ellipsoids can be compared using the metrics as described in the research paper.

Algorithm 1: Finding closest orientation and principle axis order.

foreach *trial* **do**
  Get d_{ref}, R_{ref}
  Get d_{com}, R_{com}
  Get characteristic Axis of d_{com} and d_{ref}
  Swap the index of d_{com}, R_{com} such that the characteristic of d_{com} points in the direction of d_{ref}
  This results in $R_{s,com}$ and $d_{s,com}$
  if $det(R_{s,com}) = 1$ *(valid rotation)* **then**
    continue;
  else
    swap index once more (of the axes that is not the characteristic axis producing a valid rotation)
  end
  if *reference or user ellipsoid is a circle or cigar* **then**
    rotate new $R_{s,com}$ to find closest representation;
  end
end

B.2. Experimenter GUI

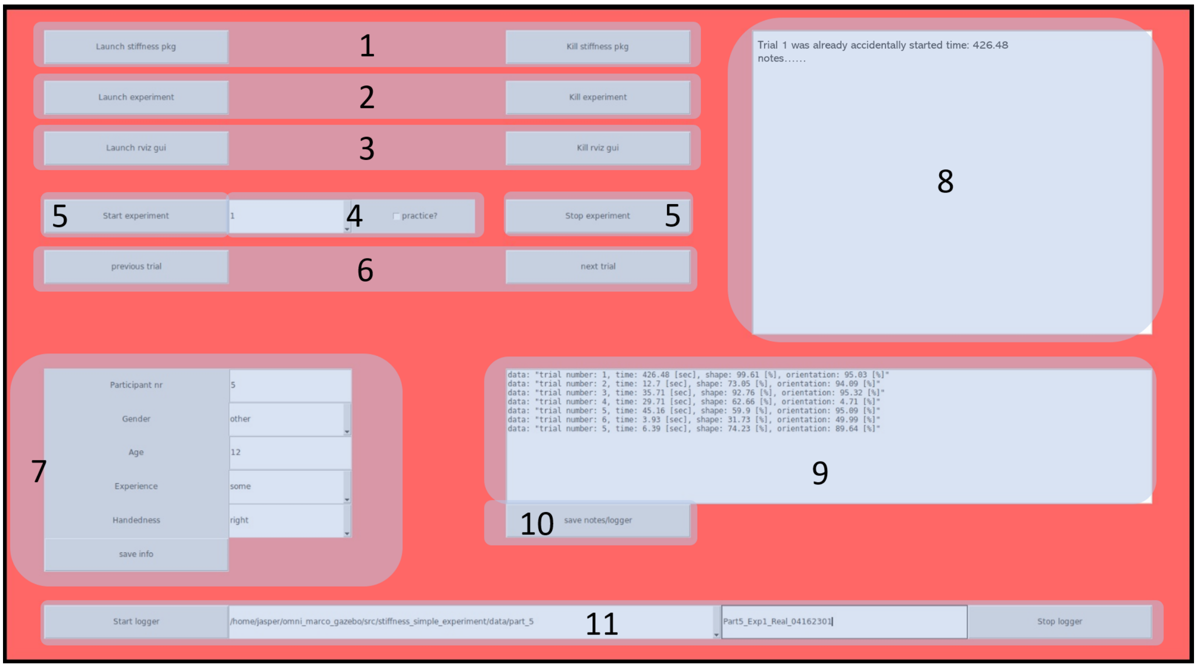

Figure B.2: Gui used by the researcher to supervise and manage the experiment.

The experimenters Graphical User Interface is launched from within the **stiffness_simpel_experiment** and used to supervise and manage the experiment, The interface is presented in Fig. B.2

1. Buttons used to launch and kill the Omni + stiffness nodes.
2. Buttons used to launch and kill the experiment node.
3. Buttons used to launch and kill the Participants Graphical User Interface B.3.
4. Drop down list and checkbox used to select the experiment.
5. Buttons to start and stop the experiment trials.
6. Buttons used to click through the trials. Would allow starting experiments from different trials in case something went wrong. Eventually only used for debugging of the experiment code.

7. Entry fields for participant information consisting of participant number, Gender, Age, teleoperation experience, if they were right or left-handed. Plus an additional button to save and create a directory to store the data from the participant and experiment. For teleoperation experience, they could choose between None, 1 hour, 10 hours, 1 day, 1 week, 10 weeks, and more.

8. Entry field used to make notations during the experiment.

9. Text field that provides the scores of the trials during the experiment. Can be used to inspect during the experiment.

10. Button used to save scores and notation of 8 and 9.

11. Buttons used to start and stop the logger. Save directory and file names are automatically generated or can be manually selected.

B.3. Participant GUI

The participants Graphical User Interface is launched from within the **stiffness_simpel_experiment** and used to provide visualization of the experiment simulation. The 2 screens launch separate instances of RVIZ. Therefore, all the click functionalities, visualizations, or any other RVIZ widgets can be viewed independently on both screens. For the experiment, all functionalities are hidden. Additionally, the buttons below the view are used to change the reference view of the experiment. This is not used during the experiment. The participant GUI with visualization can be seen in Fig. B.3. In Fig. B.4 the Omni movements show in relation to the screen.

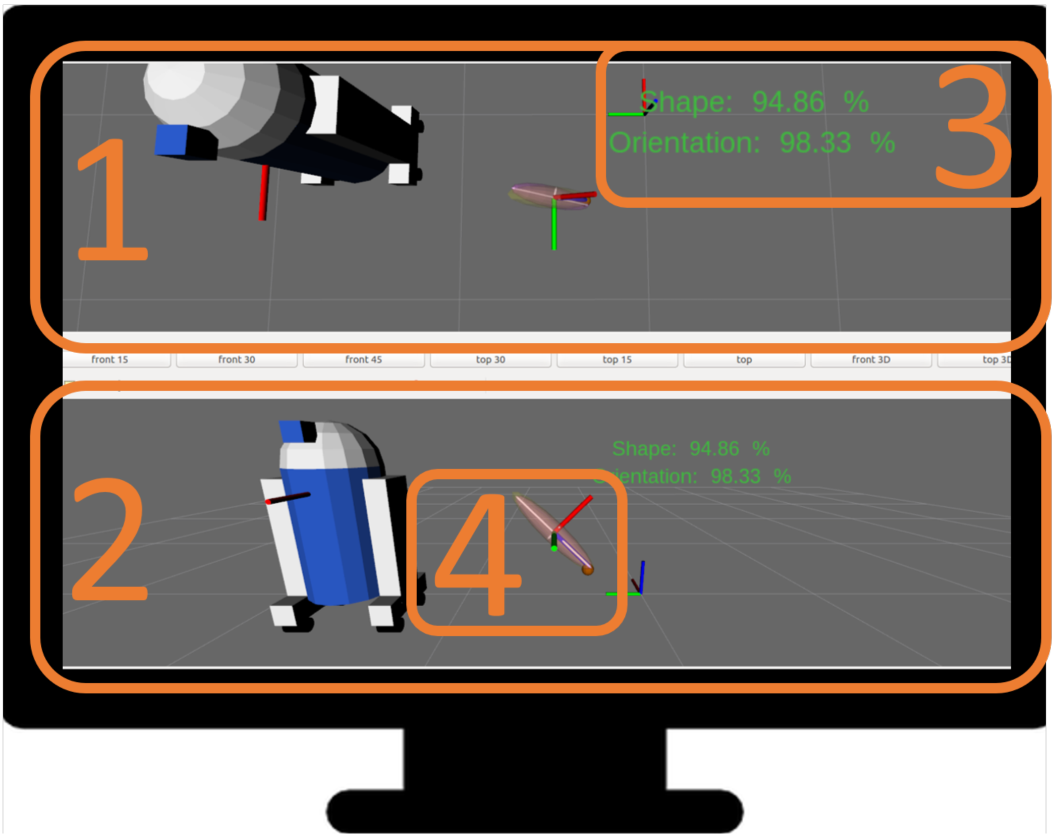

Figure B.3: 1) Top view of the experiment scene, looking down on the horizontal plane. 2) Front view of experiment scene, looking at the vertical plane. 3) Feedback scores of the trials during the experiment. 4) Reference ellipsoid (yellow) and user commanded ellipsoid (purple) visualization.

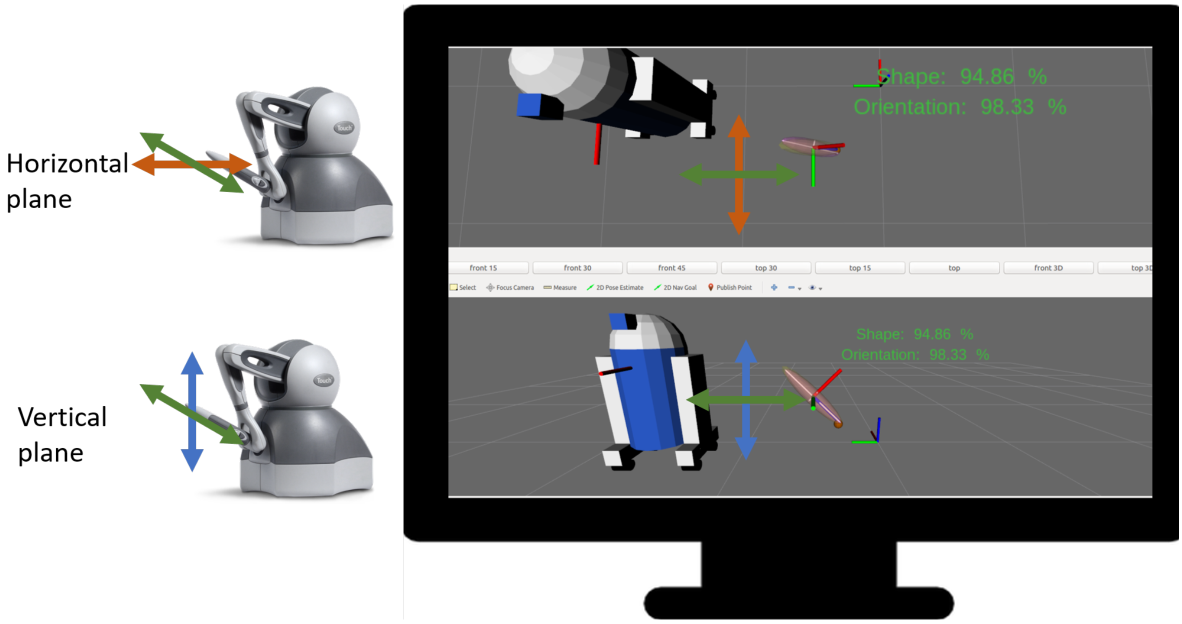

Figure B.4: Haptic device stylus movements in relation to the scene. The green arrow moves the stylus from left to right; the blue arrow move the stylus up and down; and the orange arrow moves the stylus forward and backward.

B.4. Participant feedback scores

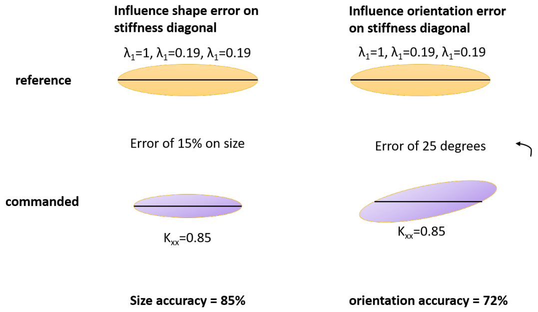

Figure B.5: This schematic illustrates the idea of how the orientation and size error influences the stiffness diagonal. Additionally, it shows how the metrics used for the experiment feedback differ

Color	Red	Orange	Green
size [%]	$score < 85$	$85 \leq score < 92.5$	$score \geq 92.5$
orientation [%]	$score < 70$	$70 \leq score < 85$	$score \geq 85$

Table B.1: Shows how the colors are set for different accuracy scores on size and orientation

The colors for the feedback scores for orientation and shape accuracy are defined to have a different range since they impact the stiffness differently. As an example, an accuracy score of 90% for the shape impacts the stiffness more than an accuracy score of 90% for the orientation. The lower bound is experimentally chosen upon the performance of the pilot study. The idea was to find a lower threshold that did not discourage the participants but also would not be too easy. The different size and orientation scores are defined such that the orientation error and shape error have approximately the same influence on the stiffness commands. This is an approximation since the orientation error of an ellipsoid is presented by a single angle however, the axis of rotation and type (1 and 2 DoF) of the compliance ellipsoid highly influence how this would contribute to the stiffness matrix diagonals. In App. C, a small analysis provides an idea of how the orientation and size influence the stiffness for 1 and 2 DoF ellipsoids.

In this case, the feedback scores are set up using the 1 DoF compliance ellipsoid en looking at the influence on the stiffness diagonal. Therefore, a shape score of 85% indicates that the stiffness diagonals have a difference of 15% with respect to the reference ellipsoid. A 15% difference on the stiffness diagonal due to an orientation error, would correspond to an angle of 25 degrees. This is illustrated in Fig. B.5. How the angle of 25 degrees corresponds to stiffness difference of $(1-0.85)$ 15% can be seen from Fig. C.2b. This plot shows how the stiffness diagonals change for given rotations. Therefore, if we convert the 25 degrees angle to an orientation accuracy score we get $(100-25)\cdot\frac{100}{90} = 72\% \approx 70\%$. This results in an orientation accuracy score of 70% and size accuracy scores of 85% that are colored red as these have approximately the same influence on the stiffness diagonal for 1 DoF stiffness commands. The shape accuracy and orientation accuracy equations are given by

$$s_{acc} = 100 - \frac{1}{n}\sum_{i=1,2,3}^{n}\left\{\frac{|\sigma_{ref,i}-\sigma_{com,i}|}{\sigma_{ref,i}} \times 100\right\} \tag{B.1}$$

and

$$\alpha_{acc} = 100 - (\alpha\frac{2}{\pi} \times 100) \tag{B.2}$$

where α is the angle in radians.

C

Influence Metrics on Stiffness and Force

This section briefly illustrated how orientation and size error influence the resulting stiffness diagonal and force. Most importantly it can be seen that for a relative size error the stiffness diagonal in/decreases linearly, while for an orientation error, the stiffness diagonals change following parts of sinusoidal curves. The plots shown in this chapter are used in determining the red feedback scores as which were presented to the operator during the user experiment. The scores can be seen in App. B.4.

C.1. Influence size

In this example, the size error is uniformly increased and scaled relative to the eigenvalues. Therefore, a 100% size match is a diagonal matrix with the values $[1, 0.19, 0.19]$, while a 0% size match has a stiffness diagonal of $[0, 0, 0]$. See the equation for the shape accuracy in (B.1). The eigenvalues are scaled between 0-1 and have the same ratio as the large reference 1 DoF "cigar-shaped" compliance ellipsoid as used for the experiment.

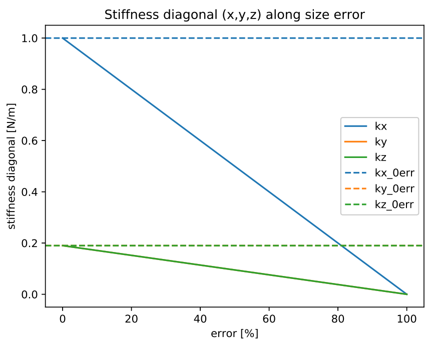

(a) Stiffness diagonal change for uniformly increasing size error Reference ellipsoid is a diagonal matrix with on the diagonals $[1, 0.19, 0.19]$.

(b) Force response for perturbation in x-direction for uniformly increasing size error.

C.2. Influence orientation

This section shows how an orientation error of $0 - 90$ degrees influences the stiffness diagonal and force response for 1 (cigar-shaped) and 2 DoF (oval-shaped) ellipsoids as used in the experiment. The 2 DoF ellipsoid is rotated around three individual axes to illustrate that rotation around different axis influence the stiffness differently.

The eigenvalues of (a) and (b) are scaled between 0 and 1 and represent the same ratio as the large reference 1 DoF "cigar-shaped" compliance ellipsoid as used for the experiment which measured $[0.45, 0.085, 0.085]$ for the axis diameters. Therefore, the reference stiffness matrix is a diagonal matrix with the eigenvalues on the diagonal. Similarly, the eigenvalues of (c) - (h) represent the "oval-shaped" ellipsoid corresponding to the axis diameters of $[0.45, 0.275, 0.085]$.

By looking at figure C.2a it can be seen that for a zero degree rotation, the eigenvalues $[1, 0.19, 0.19]$ match the stiffness diagonal. If the Ellipsoid is rotated around the z-axis, the diagonal changes following part of a sine curve. The difference between the striped line and the solid line is the error on the diagonal of the stiffness matrix. Note that if the angle is larger than 0, the stiffness matrix also has off-diagonal components that are not equal to 0. Furthermore, if the rotation would be around the x-axis, this would not have influenced the stiffness (and force response) since the z diagonal of the stiffness matrix is equal to $(0.19 - 0.19)$.

When the angle is 0, this corresponds with a perfect match in orientation with an orientation accuracy of 100% while an angle of 90 degree rotation corresponds with an 0% match inaccuracy. See the equation for the orientation accuracy in (B.2).

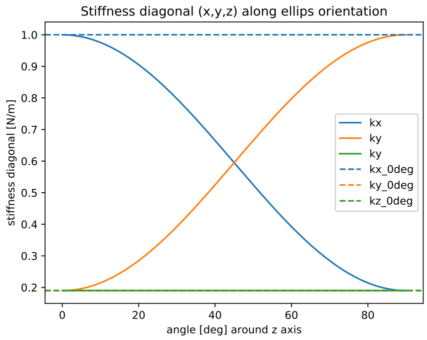

(a) Stiffness diagonal change for 1 DoF commanded ellipsoid rotated around the z-axis. Eigenvalues are [1, 0.19, 0.19].

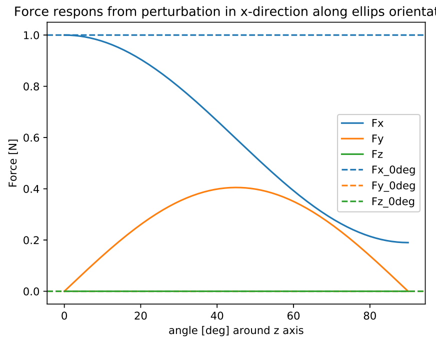

(b) Force response for perturbation in x-direction for 1 DoF commanded ellipsoid rotated around the z-axis. Eigenvalues are [1, 0.19, 0.19]

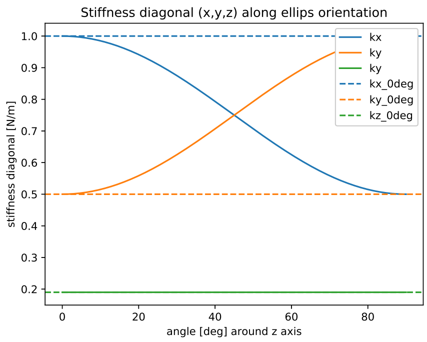

(c) Stiffness diagonal change for 2 DoF commanded ellipsoid rotated around the z-axis. Eigenvalues are [1, 0.5, 0.19].

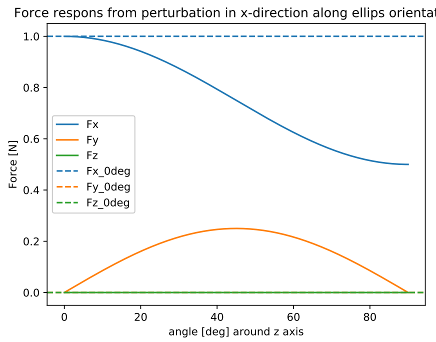

(d) Force response for perturbation in x-direction for 2 DoF commanded ellipsoid rotated around the z-axis. Eigenvalues are [1, 0.5, 0.19]

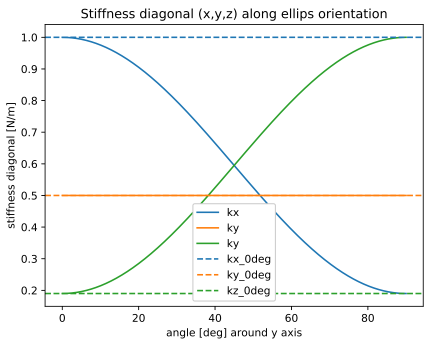

(e) Stiffness diagonal change for 2 DoF commanded ellipsoid rotated around the y-axis. Eigenvalues are [1, 0.5, 0.19].

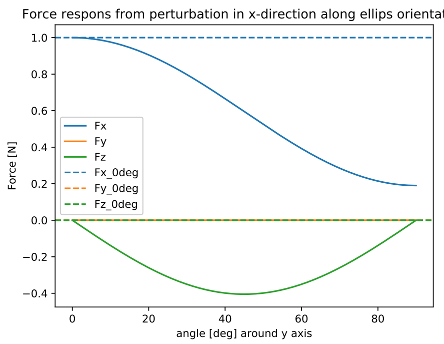

(f) Force response for perturbation in x-direction for 2 DoF commanded ellipsoid rotated around the y-axis. Eigenvalues are [1, 0.5, 0.19]

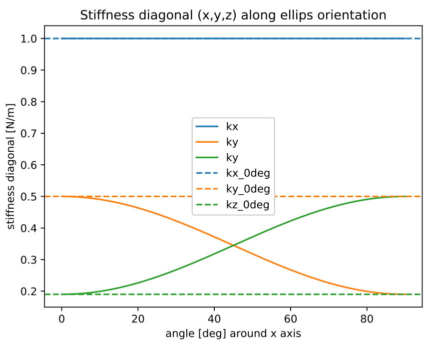

(g) Stiffness diagonal change for 2 DoF commanded ellipsoid rotated around the x-axis. Eigenvalues are [1, 0.5, 0.19].

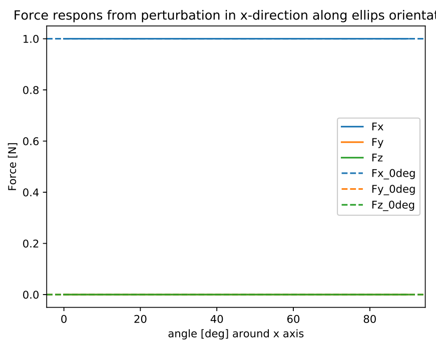

(h) Force response for perturbation in x-direction for 2 DoF commanded ellipsoid rotated around the x-axis. Eigenvalues are [1, 0.5, 0.19]

D

Pilot Study

In this section, the two pilot studies are presented. Initially, the idea was to perform two user studies experiments. The first study would check if the operator could vary the stiffness in different directions and magnitudes and would just state the performance scores. The second user study would evaluate the method for a simulated task execution.

However, the choice was made to not do a second user study but to extend the analysis of the first user study. Therefore, after the first pilot study was done, the experiment changed quite a bit. Hypotheses were setup and a questionnaire was added and the trial implementation changed. Next, a second pilot study was done to test the new implementation, procedures, and data.

The goals of the pilot studies are to get an indication of how the participants performed, if the data was generated correctly if the experimental protocol was clear, and to find out how the experiment could be improved.

D.1. Pilot 1

The following was observed from the first experiment

- 2 DoF clearly more difficult that 1 DoF, especially the orientation. Fig. D.1a
- Large shapes take more time.
- By playing back the experiment, a systematic error was observed in orientation for specific orientations.
- Some orientations more difficult than others within the condition.

Complete counterbalancing of 4 conditions would require 24 participants while Latin squared would require 16 participants. Since the experiment could only be performed with participants at the office, there were not enough participants to counterbalance with these methods. Since the pilot showed a clear difference in 1 and 2 DoF, the choice was made to always follow a 2 DoF condition after a 1 DoF condition in that same plane. Only the horizontal and vertical plane conditions were counterbalanced. Therefore, in the 2 DoF condition, the participants had already some practice.

Initially, the size of the ellipsoids was either small or large to provide some variation. However, since the metric trial time was influenced by the size, every ellipsoid was made to have a small and large size. This also allowed us to investigate the difference in size for the other metrics. Subsequently, the 2 DoF ellipsoids were redesigned to be as similar as possible to the 1 DoF ellipsoids such that they compare fairly.

Furthermore, it was observed that the position of the haptic device relative to the operator, screen, and table influenced the performance. The participant leaned over the haptic device which likely contributed to the systematic error around a specific axis

The following was improved after the first pilot

- Counterbalance the planes and not commanded DoF
- Created ellipsoids that had a large and small size

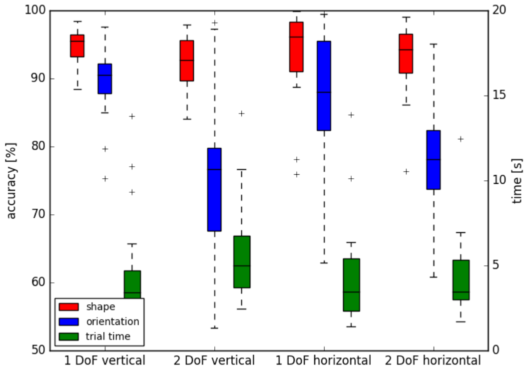

(a) Pilot results for different conditions. These results show the accuracy scores which were presented as a feedback measure to the operator. The accuracy scores (blue and red) belong the left y-axis while the trial times (green) belong to the right axis. The order of conditions were: 1 DoF vertical, 2 DoF vertical, 1 DoF horizontal, 2 DoF horizontal

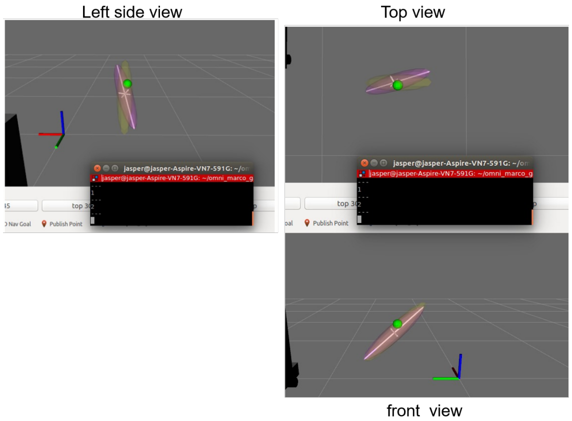

(b) By playing back the experiment (rosbag play), it was observed that the tilt around the green axis was a difficulty and had the same systematic error for this participant. This could be due to the posture of the participant with respect to the haptic device.

- Setup hypotheses to evaluate commanded plane, DoF, and size
- added van der Laan questionnaire
- after each experimental condition 2 simple questions were asked to provide a bit more insight into the method. They were asked how they feel about their performance and if everything was clear.
- The haptic device was more carefully positioned and fixed with respect to the table and screen.
- added strategy tips for commanding in 2 DoF

D.2. Pilot 2

The second pilot mainly showed that the experiment had become too long and tiring. This was solved by reducing the trials such that the experiment would be 25% shorter. Additionally, the force feedback was reduced. Finally, an extra test was implemented which participants needed to pass with sufficient scores before they were allowed to start the experiment.

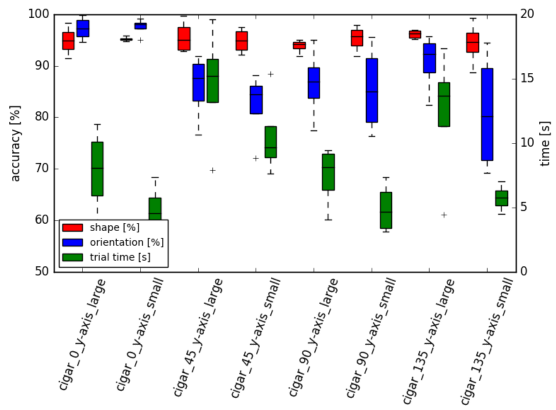

(a) Vertical plane, 1 DoF

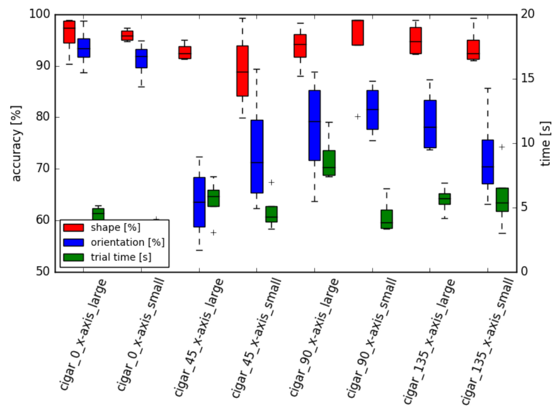

(b) Horizontal plane, 1 DoF

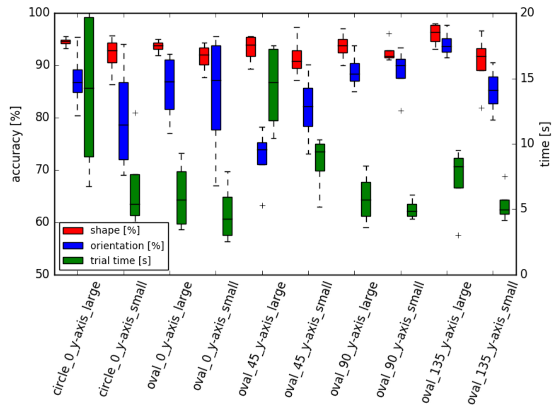

(c) Vertical plane, 2 DoF

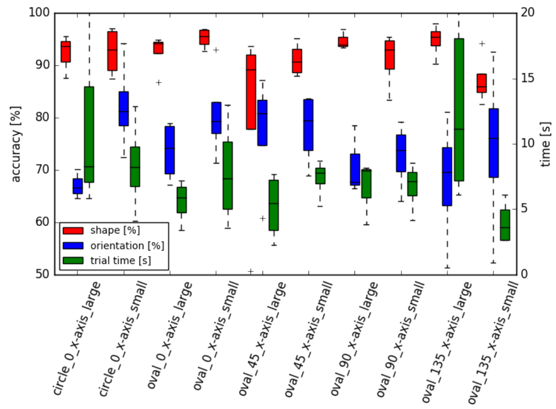

(d) Horizontal plane, 2 DoF

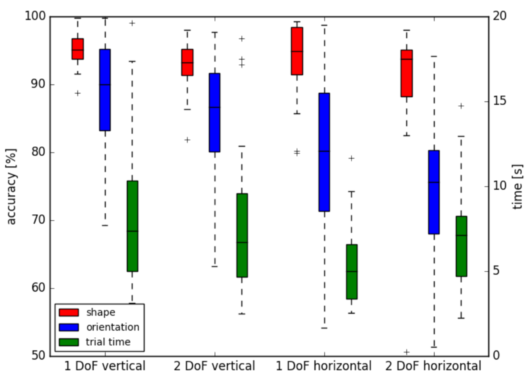

(e) All conditions. The decreasing trend in performance could be that the participant was getting tired. The order of the conditions was: 1 DoF vertical, 2 DoF vertical, 1 DoF horizontal, 2 DoF horizontal

Figure D.2: Pilot results for different conditions. These results show the accuracy scores which were presented as a feedback measure to the operator. The accuracy scores (blue and red) belong the left y-axis while the trial times (green) belong to the right axis. (a)-(d) Show the performance of the different ellipsoids. The legend reads *type-ellipsoid_rotation_rotation-axis_size*

E

Supplementary results and Data

Table E.1: The descriptive statistics (left) show the median (Q_2), first quartile (Q_1) and third quartile (Q_3) of the data sets. The Inferential statistics (right) test the H_0 hypothesis (equal medians) of the different conditions using the Wilcoxon signed-rank test. Significant values ($p \leq 0.05$) rejecting H_0 are printed in bold.

		Descriptive Statistics						**Inferential Statistics**		
Metrics\Conditions		1 DoF (493)	2 DoF (493)	Horizontal (555)	Vertical (555)	Large (556)	Small (556)	1 DoF = 2 DoF	Horizontal = Vertical	Large = Small
trial time [s]	Q_2	5.68	6.88	7.06	6.14	8.22	5.60	w = 43620	w = 62291	w = 32307.5
	Q_1	3.34	4.02	4.11	3.47	4.28	3.29	**p < 0.001**	**p < 0.001**	**p < 0.001**
	Q_3	9.72	11.74	11.51	10.75	13.90	8.75			
absolute average	Q_2	$0.92 \cdot 10^{-2}$	$1.49 \cdot 10^{-2}$	$1.25 \cdot 10^{-2}$	$1.27 \cdot 10^{-2}$	$1.63 \cdot 10^{-2}$	$0.98 \cdot 10^{-2}$	w = 34089	w = 75851	w = 71071.5
size error [-]	Q_1	$0.45 \cdot 10^{-2}$	$0.91 \cdot 10^{-2}$	$0.74 \cdot 10^{-2}$	$0.68 \cdot 10^{-2}$	$0.94 \cdot 10^{-2}$	$0.53 \cdot 10^{-2}$	**p < 0.001**	p = 0.73	**p < 0.001**
[0.14 - 0.33] [2]	Q_3	$1.65 \cdot 10^{-2}$	$2.26 \cdot 10^{-2}$	$2.16 \cdot 10^{-2}$	$2.00 \cdot 10^{-2}$	$2.55 \cdot 10^{-2}$	$1.59 \cdot 10^{-2}$			
relative average	Q_2	97.21	93.70	95.22	95.57	95.56	95.22	w = 18487	w = 70566	w = 32504
size accuracy [%] [1]	Q_1	98.65	95.91	97.48	97.67	97.50	97.72	**p < 0.001**	p = 0.14	p = 0.11
[0-100] [3]	Q_3	94.99	90.06	92.29	92.86	92.75	92.15			
orientation	Q_2	6.65	17.41	14.79	10.87	11.45	12.92	w = 15658	w = 54113	w = 66391
error [deg]	Q_1	2.98	10.83	6.56	5.20	5.71	5.84	**p < 0.001**	**p < 0.001**	**p = 0.004**
[0-90] [3]	Q_3	14.13	26.09	23.87	18.26	20.34	21.96			

[1] Different than the other metrics, high scores represent high performance.
[2] Present the minimal and maximal average size of the reference ellipsoids.
[3] Presents the range of the minimal and maximal scores.

All the other plots associated with the Table E.1 are presented below.

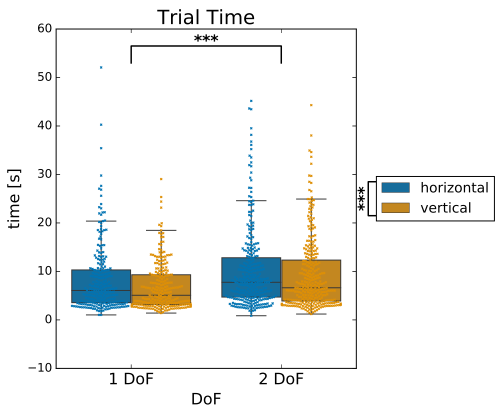

(a) Trial time versus DoF and Plane

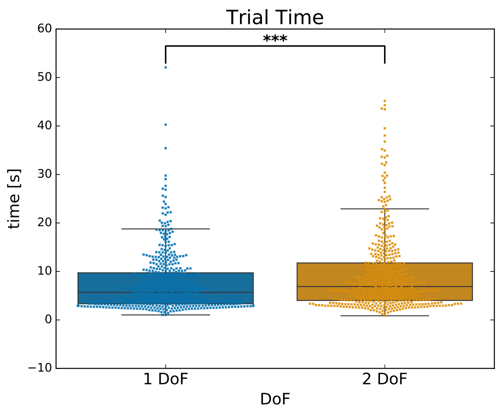

(b) Trial time versus DoF

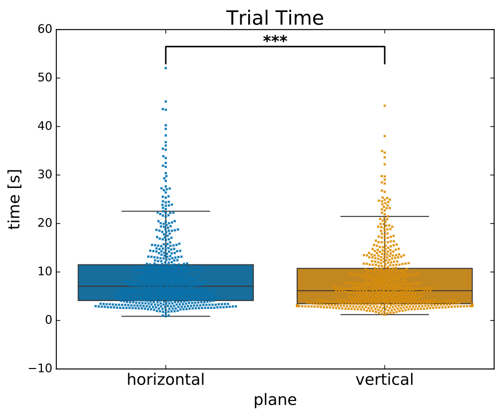

(c) Trial time versus plane

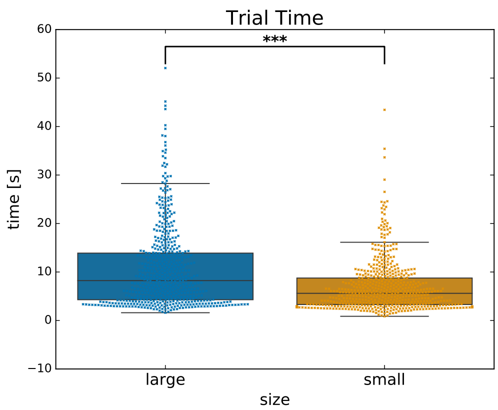

(d) Trial time versus size

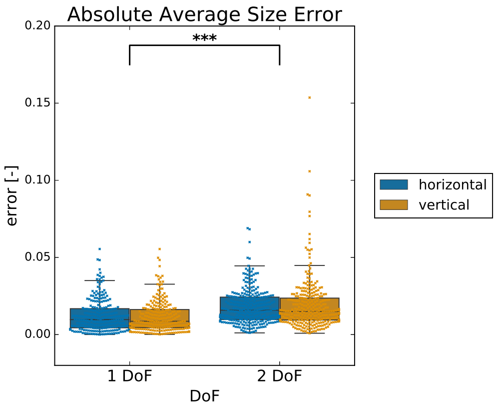

(a) absolute size error versus DoF and Plane

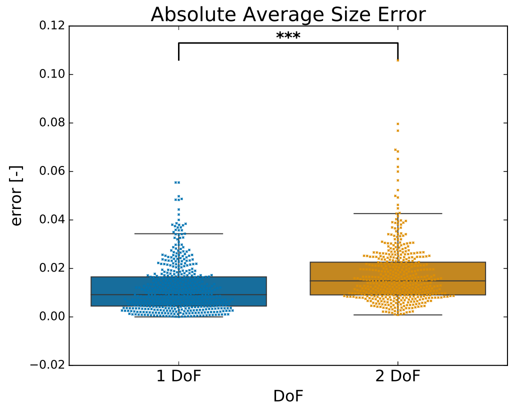

(b) absolute size error versus DoF

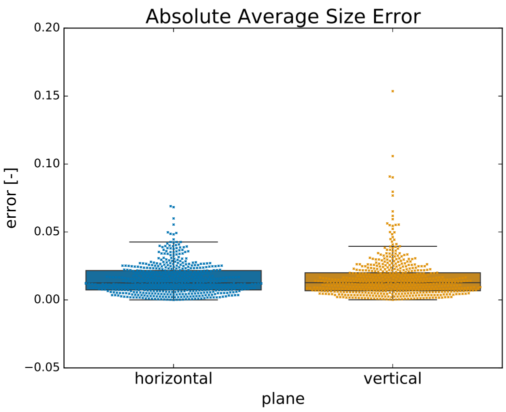

(c) absolute size error versus plane

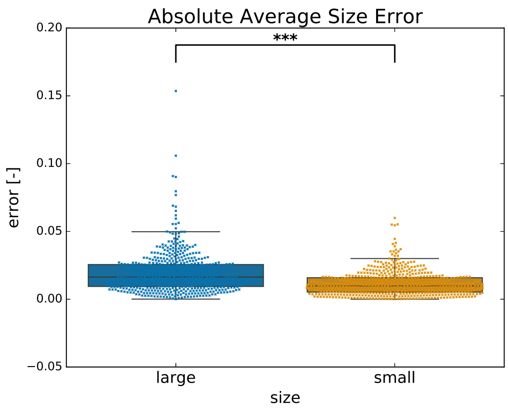

(d) absolute size error versus size

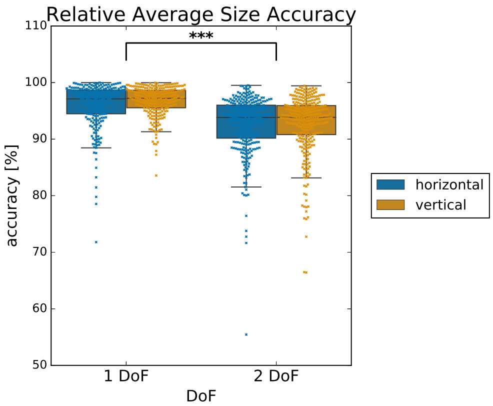

(a) relative size accuracy versus DoF and Plane

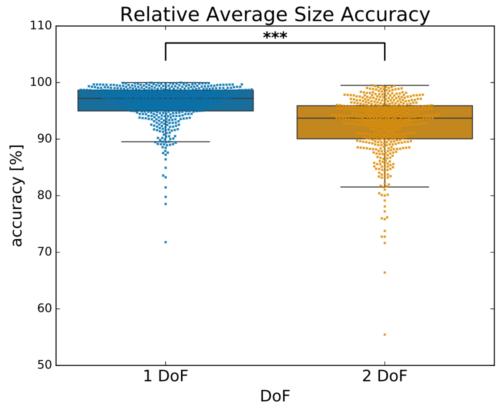

(b) relative size accuracy versus DoF

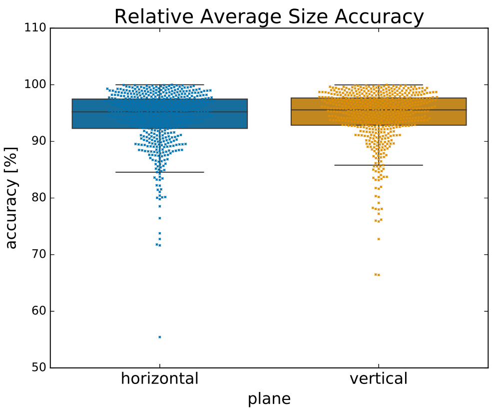

(c) relative size accuracy versus plane

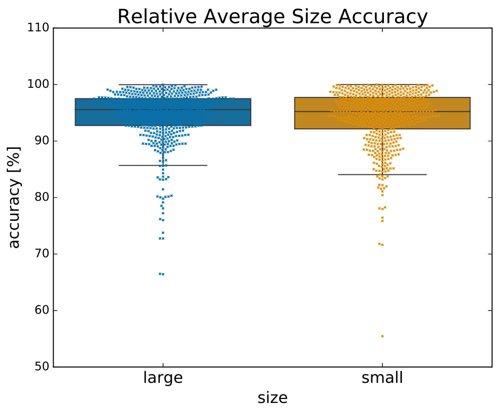

(d) relative size accuracy versus size

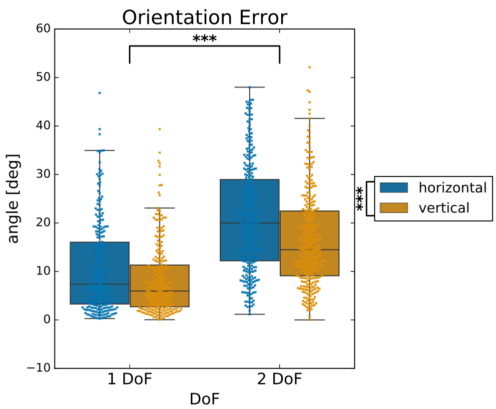

(a) orientation error versus DoF and Plane

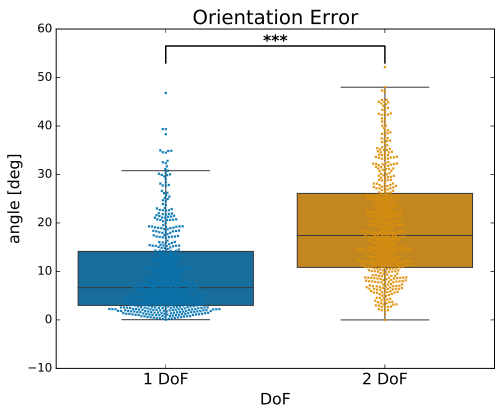

(b) orientation error versus DoF

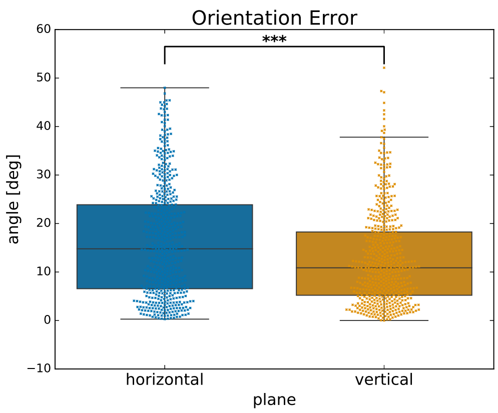

(c) orientation error versus plane

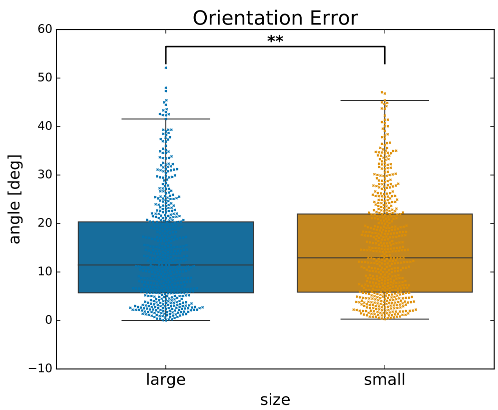

(d) orientation error versus size

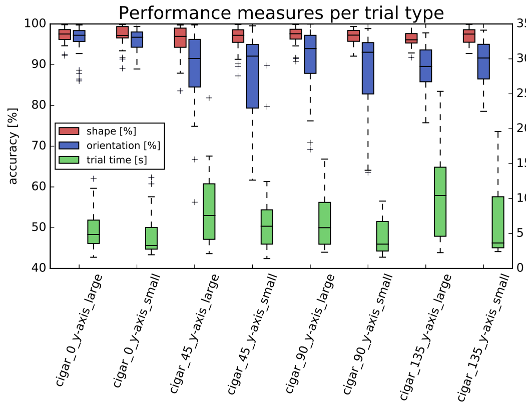

(a) Vertical plane, 1 DoF, per ellipsoid type

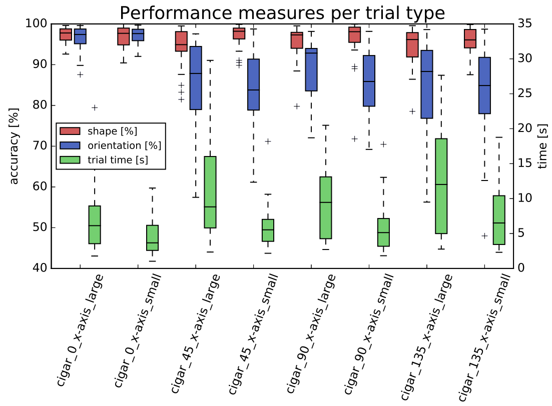

(b) Horizontal plane, 1 DoF, per ellipsoid type

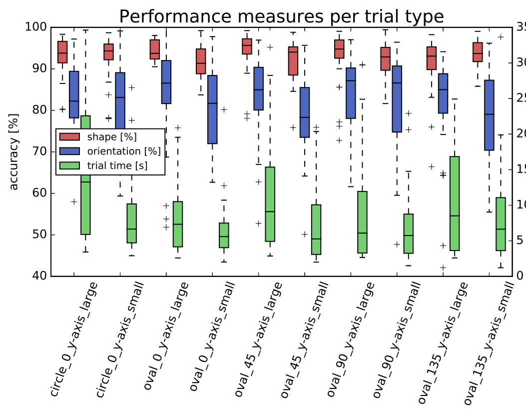

(c) Vertical plane, 2 DoF, per ellipsoid type

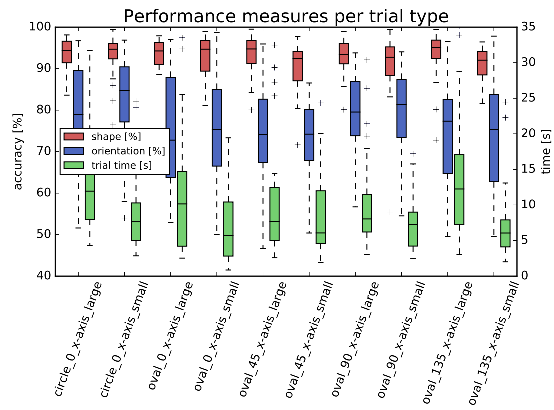

(d) Horizontal plane, 2 DoF, per ellipsoid type

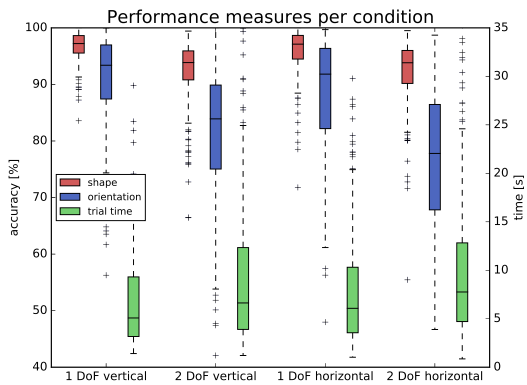

(e) All conditions

Figure E.5: The results show the accuracy scores which were presented as a feedback measure to the operator. The accuracy scores (blue and red) belong the left y-axis while the trial times (green) belong to the right axis. (a)-(d) Show the performance of the different ellipsoids of which the legend reads *type-ellipsoid_rotation_rotation-axis_size*. (e) shows the performance per condition.

F
Participant Feedback

F.1. Questionnaire feedback

Summarized participant feedback based of open questions from the questionnaire

(p) = pilot

(nr) = participant number

What did you like or found helpful?

- (P) two perspective is helpful
- (1) The interface overall is oke
- (2) Liked the way the experiment was set-up and assisted
- (3) Force feedback
- (3) Visualization of the 2 planes
- (4) Sliding window of 2 seconds was just right
- (5) For the vertical plane case, I found the commanding rather intuitive. I is easy to get the shape right in both planes but not the orientation.
- (6) Good interface, easy to use
- (7) Force feedback is very useful to help you reproduce the shape
- (8) The arrow visualization of the axis of the user commanded ellipsoid
-

What did find undesirable or hard?

- (P) Perspectives are too far apart.
- (P) Repetitive experiment
- (P) Especially using a lot of force or moving fast gets tiring
- (1) The 10 (deg) angle in the bottom view. This made it harder to see the shape in the horizontal plane since it was more difficult to check the orientation.
- (2) Commanding in 2 Dof in Front plane
- (3) Getting the orientation good was difficult, shape was easy
- (3) Figuring out how I need to move the omni when switching to different plane (condition)
- (4) Had the feeling that the forces were guiding me away from the plane
- (5) For me it was difficult to get the correct orientation, especially to fix an incorrect orientation with the shape already being made.
- (5) Method was to quit trying for the arm
- (6) bit of discomfort in arm muscles
- (7) Difficulties with the pitch control (angle around horizontal axis of frontal plane). To keep the stylus in the same plane for the horizontal conditions
- (8) Orientation mostly during 2Dof

Which condition did you find most difficult?

- (P) Horizontal view, 2Dof, circles matching the orientation in this plane and applying force is hard
- (1) Ellipse 2Dof is harder to adjust. Commands in the horizontal plane is harder

- (2) Maintaining frontal plane orientation in 2Dof was hard.
- (3) Both 2dof was hard for me. Especially in horizontal plane. Hard to switch to this plane, maybe because first learned the other one.
- (4) 2D horizontal, difficulty determining the tilt
- (5) 2 DOF horizontal. I could not get the orientation right, not even by looking at my hand.
- (6) 2 DOF commanding
- (7) 2Dof horizontal because of the pitch angle
- (8) 2 DoF horizontal plane
-

Do you have any remarks

- (P) Static ellipts that resizes when a button is pressed and can be modified with more fine detail
- (1) Add a third view from the left
- (2) None, (nicely executed experiment!)
- (3) Maybe easier when you can lock the shape and then form the orientation
- (4) -
- (5) felt that I was fighting the force-feedback a lot in trials involving larger shapes which was quit tiring.
- (6) -
- (7) Additional visuals cues indicating where marker is wrt the middle of the ellipsoid
- (8) -

F.2. Notes on feedback during experiment

Researchers notes on comments of participant and answers to the questions

- How did it go?
- Any remarks?

During the experiment

Experiment ids: [e1, e2, e3, e4, e5, e6, e7, e8]
1 Dof vertical practice = e1
1 Dof vertical real = e2
2 Dof vertical practice = e3
2 Dof vertical real = e4
1 Dof horizontal practice = e5
1 Dof horizontal real = e6
2 Dof horizontal practice = e7
2 Dof horizontal practice = e8

p1 (v,h)

e3: forcefeedback easy or hard,
e4: shrinkage can be frustrating,
e5: more difficult,
e6: getting tired and more difficult,
e7: do not like bottom view (slight angle)

p2 (h,v)

- e5:135 deg oriented ellipsoids are difficult

p3 (v,h)

- e2: strategy discovered, overshoot and wait when ellipsoid decreases
- e3: significantly more difficult
- e4: Would be nice to fix stiffness and refine
- e5: 45 degree angle took some time to get it, confused with previous perspective

p4 (h,v)

- e2: Went well, Found a way to fix the diagonal ellipsoids
- e5:diagonals challenging
- e6: Figured out how to correct for 45/135 degrees.
- e7: arm getting tired and tilt is hard to estimate which is necessary for 2D ellipsoids compared to 1D
- e8: not much improvement on last experiment

p5(v,h)

- e3:force feedback not helping,
- e4: For big shapes getting tired, for changing the orientation of ellipsoid. Stopped focussing on the orientation, but more on quickly getting the shape and clicking at the right moment when it was sort of oke.
- e6: difficult.
- e8: 45/135 degrees hardest orientation not doable

p6(v,h)

- e1: Understand how to correct by looking at other view
- e2: pressing button is annoying if it is in line the line of movement
- e4: More easy to do it right the first time then to correct if already made.
- e8: Starting to get tired.

p7(h,v)

- e1: easy, comfortable,
- e2: After a lot of success, getting to comfortable and then made a small error.
- e3: more difficult than the previous. Hard changing the orientation when looking at top screen in the foreward backward way.
- e5: comments, need to look at bottom screen, especially for 45/135 degrees.
- e6: difficult: pitch angle on 45/135 degrees is not what you think it is.
- e8: tiny bit tired to the end. If you understand what to do I feel I could get it.
- Visuals could be a bit better. get Arrows on the ball that point toward middle.

p8(v,h)

- e1: diagonal difficult,
- e2: Found strategy that works.
- e3: Choice orientation first and then make size, orientation of small shapes is difficult to see.
- e4 : Changed strategy of holding the stylus not the feeling that I am improving on this condition.
- e5: In horizontal plane, difficult to keep pitch = 0
- e6: Delay of stiffness change makes it more difficult. Smaller shapes are easier. Commanding a bit below the plane to feel the force feedback, in this way I stay better around pitch = 0.
- e7: Circles easier than ovals, harder to control pitch if you also need to control 2 axis. Delay takes some time before you see the effect.
- e8: Small ellipsoid not clearly visible. 135 degree ellipsoid difficult to position myself in a position that works

G

Experimental Procedures

The experimental procedures contain the following:

1. **Experimental protocol –** This document provides an overview of all the steps that are necessary to perform the experiment. From recruiting participants to the experiment in finished
2. **Study Information –** This document complements the consent form and will provide information regarding: purpose of study, benefits and risks, safety precautions/ procedures, withdraw procedures, data (collection, storage and usage) and contact details.
3. **Informed consent –** Document to be signed by the participant.

G.1. Experimental Protocol

Experimental Protocol

This document provides an overview of all the steps that are necessary to perform the experiment. Detailed information can be found in the **Study information, informed consent** and the **Participant instruction** forms.

1. Contacting participants

8-12 participants will be contacted via e-mail and asked if they would like to participate in the experiment. Potential participants are only people who I come in contact with and do not require travelling to participate in the experiment. These include co-workers and roommates.

They receive:

1. **Study information –** Explaining the purpose of the study, risks/ benefits, safety precautions/procedures, withdrawal procedures and data management.
2. **Informed consent –** Which can be signed when willing to participate. Either by replying to the mail or signing it upon receival of the participants.
3. **Participant instructions –** Detailed instruction of the experiment and what is expected from the participants.

2. Receiving participants

Once the participants agree to participate, they are welcomed in the office of Heemskerk Innovative Technology and reminded on the Corona related measures (e.g. wash hands) as described in the **Study information**. A small study introduction is given and the informed consent and study information is provided/ read aloud when necessary. The safety and withdrawal procedures are once again mentioned.

3. Experiment instructions

When the informed consent is signed, the participants will be seated and the experiment specifics are explained. This is done via the **Participant instructions** document. This explains the layout of the experiment, how to use the devices and how to behave during the experiment.

4. The Experiment

Before starting, information about the participant is entered on the computer (age, gender, experience, etc.). Next, the participants are allowed 5 minutes play around with the haptic device such that they know how to operate it. Subsequently, 4 tests will be performed all preceding a practice run. In between the four tests, a small break is scheduled.

5. Participants leaving

When the experiment is finished, the participants are thanked for participating and reminded to wash their hands again before leaving. Next, everything is cleaned and made ready for the next participant to enter. Enough time between the participants is scheduled such that proper cleaning of the devices is possible.

Final remarks

Participants are allowed to ask questions during the whole experimental protocol. Furthermore, at any time, participants can withdraw from participation of the experiment without having to give reason. This is also explained in the **Study information** form.

G.2. Study Information

Study information

Please read this information carefully before participating in the experiment and before signing the consent form. This document complements the consent form and will provide information regarding:

- The purpose of the study
- Contact details of researcher, data protection officer and supervisors
- Benefits and risks of participating
- Safety precautions and procedures
- Withdraw procedures
- Data collection, storage and usage

Purpose of study

Nowadays, cost-efficient health-care assistance is necessary to maintain good quality of care. Tele-operated semi-autonomous care robots employed in medical facilities aim at meeting this demand. A key requirement of such robots is to have autonomous manipulation skills suited for various tasks while operating in an unstructured environment. In order for the manipulation tasks to be successful and safe, the robotic arm is in need of varying compliant behaviour. Therefore in addition to the arm motion, it also requires interactive behaviour which is realized through stiffness commands from the operator.

In this research, a new method/setup is developed where the operator is providing stiffness commands to a care robot by teleoperation.

In this experiment you as an operator will be sending stiffness commands. This will be done in a basic experiment where the goal is to evaluate the stiffness commanding setup and method. You will be operating a haptic master device (Geomagic Touch) for providing the stiffness commands.
This experiment will approximately take 40 minutes in total where you will be performing 4 tests.

In the future, a second experiment might be done where the stiffness commanding method will be used to give commands to an actual or simulated robot performing a manipulation task. This will not be part of this experiment.

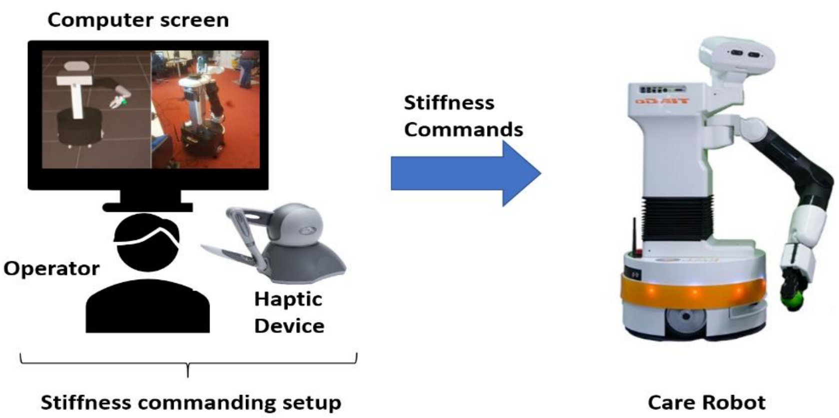

Contact details

- Researcher: Jasper Schol, jasper.schol@live.nl, +31 (0) 612267974
- University Supervisor: Prof.dr.ir. D.A. (David) Abbink, D.A.Abbink@tudelft.nl
- Company Supervisor: Cock J. M. Heemskerk, PhD, c.heemskerk@heemskerk-innovative.nl
- Data Steward: Y. Türkyilmaz-van der Velden, Y.Turkyilmaz-vanderVelden@tudelft.nl

Benefits and risks

There are no direct personal benefits by participating in this experiment. The risks of the experimental setup are:

- Discomfort of staring to a screen
- Physical discomfort from holding the stylus of the Geomagic Touch. The forces the Geomagic Touch can deliver are small (up to 3.3 Newton). This can lead fatigued muscles or an uncomfortable posture/positioning.
- Contamination of COVID-19. To prevent contamination of COVID-19 extra precaution are made and explained in the safety precautions and procedures section.

Safety precautions and procedures

Experiment

- The Geomagic Touch can be turned off by the researcher and the participant.
- Participants are seated comfortably and asked about injuries that could interfere with the physical activities that come with moving the stylus.
- To prevent fatigued muscles or discomfort, 5 minute breaks are scheduled in between the four tests.

Covid-19

To prevent contamination of the corona virus, the following precautions are made. These comply with the regulations set by the RIVM and are upheld during the whole experiment. The researcher will keep up to date with regulations.

- The participants and researcher should not have any symptoms relating to the coronavirus now, or in the past 2 weeks. Additionally both researcher and participant should not live with people that do have symptoms and/or are quarantined.
- Participation in the experiment should not require additional travelling.
- When arriving and leaving both the researcher and participant must wash their hands with soap.
- A distance of at least 1.5 meter should be maintained at all times.
- Only three people are allow in one room at the same time.
- The devices that are used, are thoroughly cleaned with disinfecting alcohol wipes.
- All the objects the participants might be in contact with are cleaned with soap or disinfected with alcohol wipes.
- The researcher will keep up to date with the regulations set by the RIVM to ensure they are upheld during the whole experiment.

Withdrawal procedures

Participation in this experiment is on a voluntarily basis. You can refuse to answer questions and you can withdraw from the study at any time. There is no need to give reason and this will not have any negative consequences.

Data collection, storage and usage

The only direct personal identifiable data that is collected will be name and signature on the informed consent. This will not be coupled to other personal data gathered in the experiment. Other personal data that will be gathered is age, gender, dominant hand and former experience with teleoperation. This will only be shown in aggregated form in the master thesis. The researcher (myself), my professor (David Abbink) and one company employees (Jelle Hofland) will have access to the data gathered which will be stored on the project storage drive at the TU Delft for 10 years.

G.3. Informed Consent

Consent Form for participating in a tele-operated stiffness commanding method

Please tick the appropriate boxes	**Yes**	**No**
Taking part in the study		
I have read and understood the study information dated 17/07/2020, or it has been read to me. I have been able to ask questions about the study and my questions have been answered to my satisfaction.	○	○
I consent voluntarily to be a participant in this study and understand that I can refuse to answer questions and I can withdraw from the study at any time, without having to give reason.	○	○
I understand that taking part in the study involves capturing and storing of **non**-direct personal identifiable data as well as this consent form containing my name and signature. Data gathered will not be linked to this consent form such that results are anonymous. The data will be stored according to the TU Delft Research Data Framework Policy. https://www.tudelft.nl/en/library/current-topics/research-data-management/	○	○
Risks associated with participating in the study		
I understand that taking part in the study involves the following risks: • Contamination of Covid-19 • Physical discomfort of staring to a screen • Physical discomfort from holding the stylus of the haptic device (Geomagic Touch)	○	○
Use of the information in the study		
I understand that information I provide will be used for the analysis during the graduation project. The non-direct personal identifiable data and master thesis will be uploaded to the TU-Delft repository and the companies repository such that knowledge can be shared among other students, researchers and company personnel.	○	○
I understand that personal information collected about me in this consent form, will not be shared beyond the study team and stored at the private TU-Delft Project Storage system only.	○	○
Future use and reuse of the information by others		
I give permission for the non-direct personal identifiable data that I provide to be archived in the Project Storage system of the TU-Delft and the 4TU Center for research, such that it can be used for future research and learning.	○	○

Signatures

______________________ ______________________ ________

Name of participant [printed]

Signature Date

I have accurately read out the information sheet to the potential participant and, to the best of my ability, ensured that the participant understands to what they are freely consenting.

________________________ ________________________ ________

Researcher name Signature Date

Study contact details for further information:

Name: Jasper Schol

Tel nr: +31 (0)6 12 26 79 74

E-mail: jasper.schol@live.nl

H

Participant Instructions

Participant Instructions

Today, you will take the role of an operator who has to try out a new setup, that is used to send stiffness commands to the care robot. Before commanding stiffness to an actual robot, our first interest is to see how this setup behaves and if people are able to use this method to command stiffness. Therefore, the goal of this experiment is to evaluate if the operator controlling the system can command stiffness variations.
In this experiment, the operator is asked to recreate a given stiffness profile by moving the stylus of the haptic device. The stiffness profile is visualized in the form of an ellipsoid and can be felt through force feedback by operating the haptic device. By comparing the operator commanded stiffness ellipsoid with the given stiffness ellipsoid, the trials are evaluated. The operator is expected to recreate the given stiffness profile as accurately as possible (but in a timely manner). Thereby emphasizing accuracy over speed.
This document will explain the experiment specifics, how to use the equipment, how to command stiffness and how to perform the experiment.

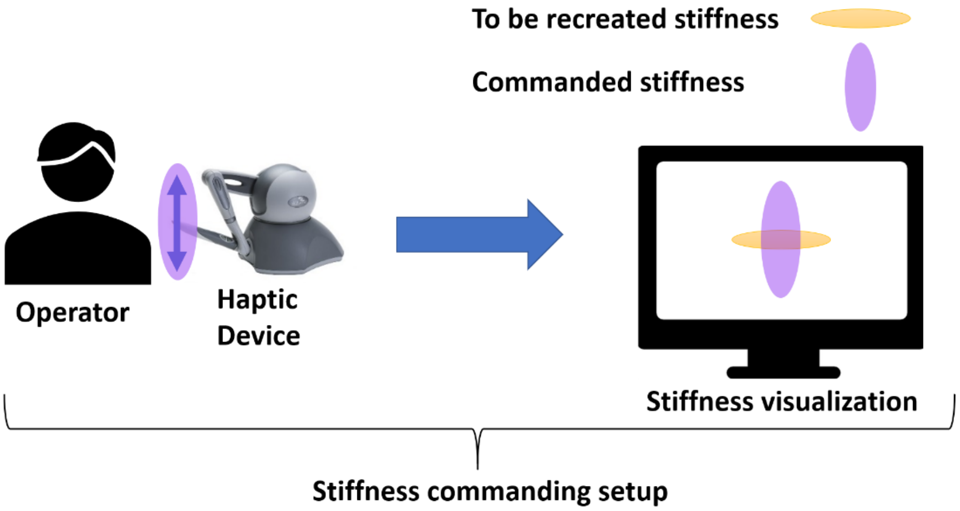

Experiment overview

The experiment will approximately take 30-40 minutes consisting of 4 conditions.

- First the operator (you), will be presented with the setup where you will receive information on how to handle the equipment and interpret the simulation. Next 12 familiarization trials are performed and once all are passed sufficiently, the first practice condition will start.
- For each of the four conditions, you will start of by performing a practice run to familiarize yourself with this specific condition (2,5 min). This is followed with the real test (2,5 min). In between the 4 conditions, a short break is scheduled (5 min).

Apparatus

- Haptic device (geomagic Touch), used to create stiffness commands and receive force feedback. Button 2 is used to (de-)activate the force feedback and button 1 is used to advance to the next trial.
- A computer screen, to visualize the simulation stiffness commands and trials.

User interface

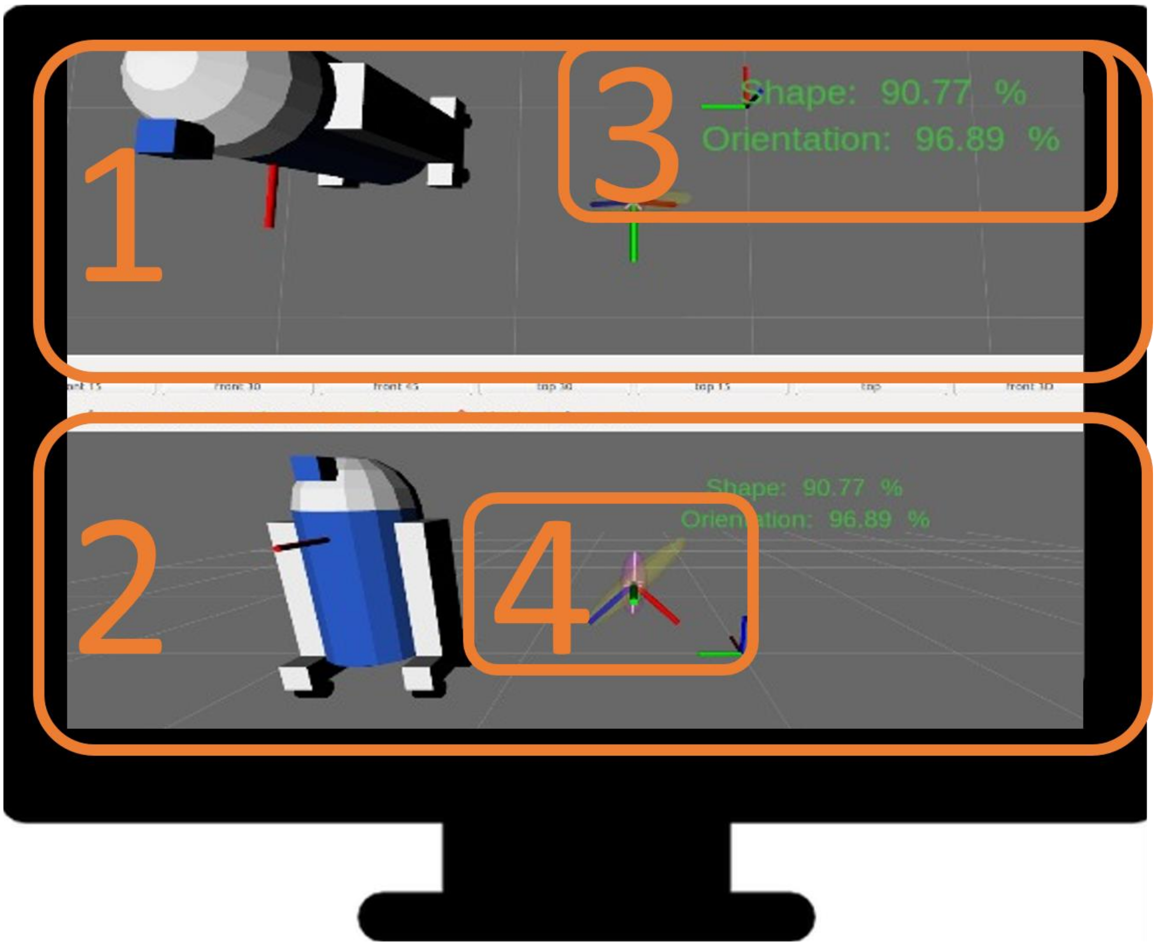

The user interface has 4 important regions to consider.

1. The **top view** of the simulation, looking down at the **horizontal plane**
2. The **front view** of the simulation, looking at the **vertical plane**
3. **Feedback text** on trial success. The scores range from 0-100% where 100% is considered perfect trial. The scores will be displayed in Green, orange or red. Where Green is considered good, orange reasonable and red score should be avoided.
4. **Stiffness visualization** of the operators stiffness and the reference stiffness profiles in the form of an three dimensional ellipsoid.

Commanding of stiffness

Stiffness is commanded by moving the stylus of the haptic device. This can be done in two ways:

1. **One dimensional commanding**. This requires wiggling the stylus along one axis (e.g. up-down). This results in a three dimensional cigar shaped ellipsoid
2. **Two dimensional commanding**. This requires making circular motions in a plane. This results in a three dimensional flattened oval shaped ellipsoids, similar to a pancake.

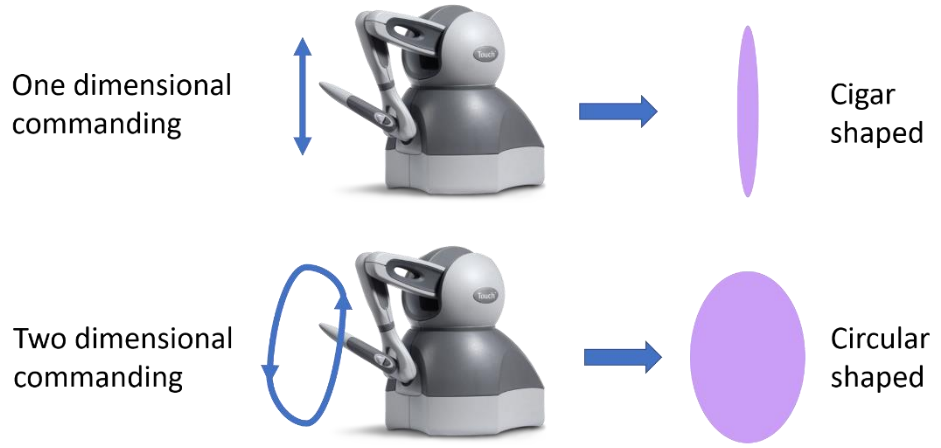

Additionally, the stylus can be moved in three dimensions. Which is grouped in commanding in **vertical plane** and commanding in **horizontal plane**.

1. Moving the stylus **up/down and left/right** is considered commanding in **vertical plane** and relates to the front view of the simulation
2. Moving the stylus **forward/backward** is considered commanding in **horizontal plane** and relates to the top view of the simulation

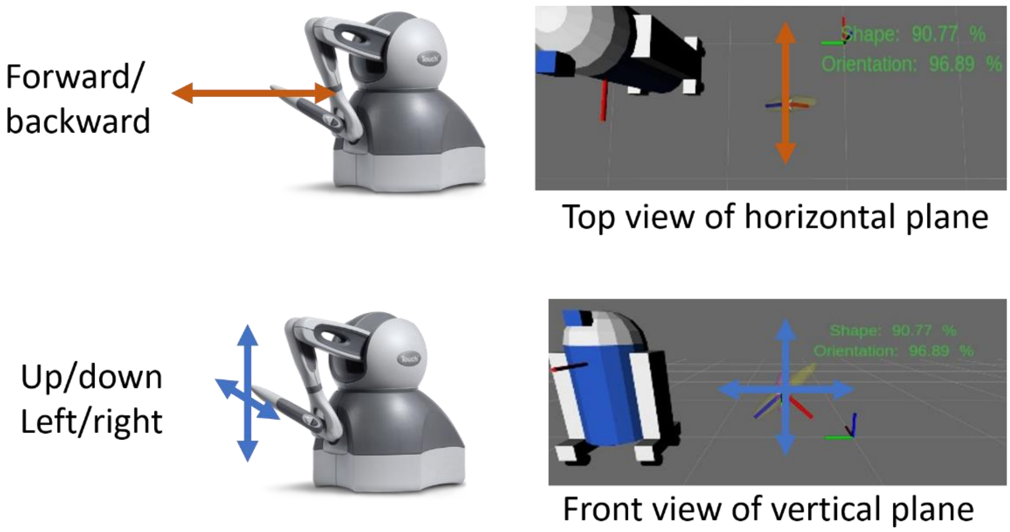

Experimental conditions and trials

There are 4 experimental conditions where different shapes in different direction should be commanded. One test is done for each condition and a practice run precedes each test.

1. The first test requires **one dimensional** commanding in a **vertical plane.** The test consist of **32 trials.**
2. The second test requires **two dimensional** commanding in a **vertical plane.** The test consist of **40 trials.**
3. The third test requires **one dimensional** commanding in **horizontal plane.** The test consist of **32 trials.**
4. The fourth test requires **two dimensional** commanding in **horizontal plane.** The test consist of **40 trials.**

Participant behaviour and Feedback

As operator, the goal is to recreate the given stiffness ellipsoid as accurately as possible (but in a timely manner). Feedback of your trial success will be presented after each trial. Trial success depends on the following two measures.

1. Shape accuracy
2. Orientation accuracy

The shape accuracy will decrease when the shape error increases. Similarly, the orientation accuracy decreases when the orientation error increases. Both shape and orientation accuracy scores can range between 0-100% where 100% indicates a perfect score. Additionally, the scores will be displayed in green, orange and red. Where Green is considered a good trial and what the operator should try to accomplish. Red trials should be avoided and orange trials indicate that there is room for improvement but performance should not deteriorate.

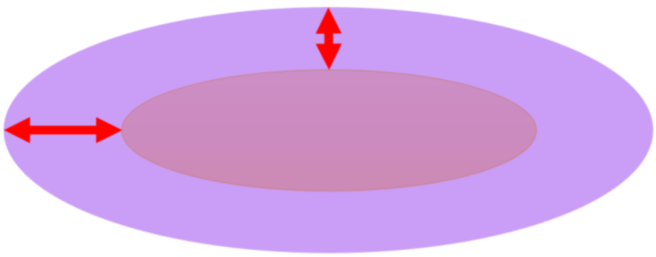

Shape error

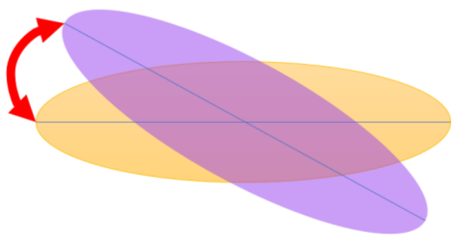

Orientation error

I

Questionnaire

Participant questions

Participant number:

What is your overall judgement of the stiffness commanding interface. Please indicate below.

1. useful	☐	☐	☐	☐	☐	**useless**
2. pleasant	☐	☐	☐	☐	☐	**unpleasant**
3. bad	☐	☐	☐	☐	☐	**good**
4. nice	☐	☐	☐	☐	☐	**annoying**
5. effective	☐	☐	☐	☐	☐	**superfluous**
6. irritating	☐	☐	☐	☐	☐	**likeable**
7. assisting	☐	☐	☐	☐	☐	**worthless**
8. undesirable	☐	☐	☐	☐	☐	**desirable**
9. raising alertness	☐	☐	☐	☐	☐	**sleep-inducing**

What did you like or found helpful?

What did you find undesirable or hard?

Which condition did you find most difficult and why?

Do you have any remarks?

Bibliography

[1] *Touch.* [Online]. Available: https://www.3dsystems.com/haptics-devices/touch/specifications.

[2] *Tiago - pal robotics: Leading service robotics*, Sep. 2020. [Online]. Available: https://pal-robotics.com/robots/tiago/.

[3] T. Foote, "Tf: The transform library", in *Technologies for Practical Robot Applications (TePRA), 2013 IEEE International Conference on*, ser. Open-Source Software workshop, Apr. 2013, pp. 1–6. DOI: 10.1109/TePRA.2013.6556373.

[4] S. Chitta, E. Marder-Eppstein, W. Meeussen, V. Pradeep, A. Rodríguez Tsouroukdissian, J. Bohren, D. Coleman, B. Magyar, G. Raiola, M. Lüdtke, and E. Fernández Perdomo, "Ros_control: A generic and simple control framework for ros", *The Journal of Open Source Software*, 2017. DOI: 10.21105/joss.00456. [Online]. Available: http://www.theoj.org/joss-papers/joss.00456/10.21105.joss.00456.pdf.

[5] B. Siciliano and O. Khatib, "Springer handbook of robotics", in. Springer, 2016, ch. Force Control, pp. 195–218.

[6] K. Kronander and A. Billard, "Online learning of varying stiffness through physical human-robot interaction", in *2012 IEEE International Conference on Robotics and Automation*, Ieee, 2012, pp. 1842–1849.

[7] P. Song, Y. Yu, and X. Zhang, "A tutorial survey and comparison of impedance control on robotic manipulation", *Robotica*, vol. 37, no. 5, pp. 801–836, 2019. DOI: 10.1017/S0263574718001339.

[8] *Wiki.* [Online]. Available: http://wiki.ros.org/rviz.